Thermodynamic study of binary systems containing sulphur dioxide and nitric oxide: measurements and modelling

Benoit Creton, Carlos Nieto-Draghi, Theodorus de Bruin, Véronique Lachet, Elise El Ahmar, Alain Valtz, Christophe Coquelet, Silvia Lasala, Romain Privat, Jean-Noël Jaubert

Thermodynamic study of binary systems containing sulphur dioxide and nitric oxide: measurements and modelling.

Benoit Creton*, Carlos Nieto-Draghi, Theodorus de Bruin,

IFP Energies nouvelles, 1 et 4 avenue de Bois-Préau, 92852 Rueil-Malmaison, France.

Véronique Lachet

IFP Energies nouvelles, 1 et 4 avenue de Bois-Préau, 92852 Rueil-Malmaison, France.
Laboratoire de Chimie Physique, Université Paris-Sud, UMR 8000 CNRS, Orsay, France.

Elise El Ahmar, Alain Valtz, Christophe Coquelet,

MINES ParisTech, PSL - Research University, CTP - Centre Thermodynamique des Procédés, 35 rue Saint Honoré, 77300 Fontainebleau, France.

Silvia Lasala, Romain Privat, Jean-Noël Jaubert

Université de Lorraine, Ecole Nationale Supérieure des Industries Chimiques, Laboratoire Réactions et Génie des Procédés (UMR CNRS 7274), 1 rue Grandville, 54000 Nancy, France.

Abstract

In this study, the thermodynamic behaviour of NO + SO_2 mixtures has been investigated by means of molecular simulation, experiment and equation of state modelling. Quantum chemical calculation were performed to investigate possible chemical reactions between NO and SO_2. Molecular simulations were based on Monte Carlo and Molecular Dynamics techniques using force fields available in the literature. Validation of simulated vapour liquid data for NO + SO_2 binary mixtures was performed on the basis of proposed new experimental data, and new sets of parameters were optimized for the PPR78 EoS. We then moved our focus on the solubility of some gases (SO_x, NO_x, CO_2, O_2, N_2) in water and brines studied by molecular simulations. We first compared performances of some combinations of salt and water intermolecular potentials in terms of

*Corresponding author: benoit.creton@ifpen.fr

density and osmotic pressure predictions. We then studied the evolution of Henry constant values for gases in brines considering various salt concentrations and temperatures.

Keywords:

Sulphur dioxide, Nitric oxide, Brine, Molecular simulation, Experiment, EoS modelling

---

SYMBOLS AND ACRONYMS

γ-ϕ	Activity-fugacity
BE	Bonding energy
CCS	Carbon Dioxide Capture and Storage
CoM	Centre of mass
E_{elec}	Electronic energy
EoS	Equation of State
EPM2	Rescaled Elementary Physical Model
f	Fugacity
GC	Gas Chromatograph
GHGs	Greenhouse Gases
HMCMD	Hybrid Monte Carlo Molecular Dynamics
IRC	Intrinsic Reaction Coordinate
K_H	Henry constant
k_{ij}	Binary interaction parameters
K_S	Sechenov constant
LJ	Lennard-Jones
m	Molality
MAE	Mean Absolute Error
MC	Monte Carlo
MD	Molecular Dynamics
N	Number of particles
NpT	Isobaric-isothermal ensemble
P	Pressure
PR	Peng-Robinson
P^{sat}	Vapour pressure
RMS	Root Mean Square
SPC/E	Extended Simple Point Charge
T	Temperature
TCD	Thermal conductivity detector
TIP4P/2005	Transferable Intermolecular Potential with 4 sites
U_{disp}	Dispersion interactions
U_{elec}	Electrostatic energy
U_{rep}	Repulsion interactions
VL	Vapour liquid
ZPE	Zero-point energy

1. Introduction

Facing the problem of global warming, many industrialized countries recently agreed in reducing their greenhouse gases (GHGs) emissions [1]. Industrial activities involving the combustion of fossil resources are responsible for a large part of the human induced carbon dioxide (CO_2) emissions. Various options have been already proven technically feasible to regulate anthropogenic CO_2 emissions to the atmosphere, and among them the carbon dioxide capture and storage (CCS) appears as a transitional key technology [2]. CO_2 can be stored in depleted geological reservoirs or deep saline aquifers [3, 4, 5]. Due to its origin and despite performed treatments, the injected CO_2 stream may contain small amounts of associated gaseous components such as O_2, N_2, SO_x, NO_x, as well as traces of noble gases [5, 6]. Varying amounts of such gas impurities in the CO_2 stream may induce more or less pronounced changes of the gas mixture properties, thus impacting the design and operation of CCS industrial units [6, 7, 8, 9]. Additionally, CO_2 and associated gases may react with subsurface components (brine, reservoir rocks, cap-rocks...) under certain salinity values, temperature and pressure conditions, affecting the long-term behaviour of the CO_2 containing mixture injected within storage sites.

The use of reactive-transport codes to investigate various scenarios is of upmost interest [10, 11, 12]. In most of the geochemical codes, chemical reactions and their equilibria are related to classical mass action laws, and water-gas equilibria are generally treated using a dissymmetrical approach γ-ϕ (*i.e.*, activity-fugacity) wherein the Henry constant (K_H) of gas species is a key property. Note that these calculations involve the use of an equation of state (EoS), and the Peng-Robinson (PR) EoS is usually used in geochemical codes [13]. EoS settings, more precisely binary interaction parameters (k_{ij}), are determined from regressions on available experimental data. The precise knowledge of the thermodynamics behaviour for binary mixtures containing: (i) CO_2 and impurities (ii) and impurities with one another, in CCS operation conditions – temperatures ranging from 218 K to 423 K and pressures up to 50 MPa [14], is necessary

to make accurate predictions using reactive-transport codes. Recent literature reviews have highlighted a wide disparity in the experimental knowledge for such binary gas mixtures [14, 15, 16, 17]. For instance, binary systems containing CO_2 and oxygen (O_2) have been largely studied while there is only scarce information on binary systems containing sulphur dioxide (SO_2) and nitric oxide (NO).

Molecular simulation techniques have been proven as cost-efficient alternatives to experimental measurements, especially when hazardous compounds and/or extreme pressure or temperature conditions are considered. These last years, we have devoted much effort to the use of molecular simulation techniques to predict vapour-liquid (VL) equilibria and transport properties for binary mixtures containing CO_2 and impurities and impurities with one another, within the different CCS stages [6, 7, 17, 18, 19, 20, 21]. Lachet *et al.* and Creton *et al.* have generated using Monte Carlo (MC) molecular simulations, data for CO_2 + SO_2 binary mixtures for temperatures ranging from 263 K to 333 K and pressures up to 9 MPa [6, 19]. Lachet *et al.* and Bourasseau *et al.* have studied using Gibbs ensemble MC coupled with the reactive ensemble, the behaviour of CO_2 + NO_x mixtures [18, 21]. Simulated data were obtained for CO_2 + N_2O binary mixtures and CO_2 + NO binary mixtures for temperatures ranging from 253 K to 293 K and pressures up to 11 MPa, and considering the chemical equilibrium $2NO \rightleftharpoons N_2O_2$ [21]. Authors have demonstrated that for CCS operation conditions of temperatures, only the monomer (NO) form exists. Bourasseau *et al.* have studied the CO_2 + NO_2/N_2O_4 reacting system considering the equilibrium $2NO_2 \rightleftharpoons N_2O_4$, for temperatures ranging from 300 K to 330 K and pressures up to 7 MPa [18]. Some simulated data were also proposed for CO_2 + Ar binary mixtures for temperatures ranging from 248 K to 288 K and pressures up to 13 MPa [6]. Creton *et al.* also reported simulated data for (i) CO_2 + O_2 binary mixtures for temperatures ranging from 233 K to 273 K and pressures up to 12 MPa, (ii) and CO_2 + N_2 binary mixtures for temperatures ranging from 220 K to 273 K and pressures up to 17 MPa [6]. Simulated phase envelopes have been also proposed for binary systems of impurities with one

another, and El Ahmar *et al.* studied SO_2 + N_2 binary mixtures and SO_2 + O_2 binary mixtures for temperatures ranging from 323 K to 413 K and pressures up to 85 MPa [20].

In the present work, we first propose new insights for SO_2 + NO binary systems by means of experimental and molecular simulation techniques. Afterwards, settings of an EoS are optimized on the basis of VL equilibrium data. New experimental VL equilibrium data are proposed and compared to data obtained with Monte Carlo molecular simulations for temperatures ranging from 273 K to 345 K. Generated MC simulation data are used to optimize sets of parameters for a PR based EoS. We then propose a comparison of various combinations of intermolecular potentials to mimic brines behaviour using molecular simulation, and provide some simulated Henry constant values in water and in brines for a series of gases including SO_2 and NO.

2. Materials and methods

2.1. Materials, apparatus and experimental procedure

Sulphur dioxide (SO_2, CAS number: 7446-09-5) and nitric oxide (NO, CAS number: 10102-43-9) were supplied by Air Liquide with a certified purity higher than 99.9 vol% and 99 vol%, respectively (Table 1). No additional purification was performed before use, except for careful degassing.

The apparatus was designed based on a "static-analytic method" and is similar to the one previously used for measurements of equilibrium properties of CO_2 + NO mixtures [22]. Two capillary ROLSI® samplers (Armines patents) [23] are available to sample liquid and vapour phases. The cell volume is about 30 ml and it can be operated up to 473 K. The equilibrium cell is made of a sapphire (aluminium oxide Al_2O_3) tube (maximum pressure 10 MPa) between two Hastelloy flanges. With the sapphire tube, we have the possibility to see the mixture at equilibrium conditions. A magnetic Hastelloy stirrer driven by an adjustable speed external system is placed inside the cell in order to speed up the reaching of the thermodynamic equilibrium.

Table 1: Chemical sample. GC stands for gas chromatograph.

Chemical name	CAS number	Source	Initial purity (weight %)	Analysis method
Sulphur dioxide	7446-09-5	Air Liquid	≥99.9	GC
Nitric oxide	10102-43-9	Air Liquid	≥99	GC

The sapphire cell is totally immersed in a liquid bath which keeps the temperature stable to ±0.1 K. The cell is equipped with two platinium probes in order to obtain a precise measure of the temperature (±0.02 K). The pressure in the cell is measured by a pressure transducer with an accuracy of $\pm 6.10^{-4}$ MPa. The pressure transducer and temperature probes are connected to a HP data acquisition unit (HP34970A). The HP data acquisition unit is connected to a computer through a RS232 interface. The sample extracted from the cell are sent to a gas chromatograph (GC) for compositional analysis. The used GC is the Shimadzu GC-2014 equipped with a thermal conductivity detector (TCD), which is calibrated for the studied compounds. The calibration of the TCD is made by introducing known pure component volumes with appropriate GC syringes. Accuracies regarding mole numbers are ±1% for NO and ±0.8% for SO_2. The maximum standard uncertainty on liquid and vapour mole fractions (Umax(x,y)) is 0.004. The HayeSep D (80/100 mesh 2m X 1/8'' silcosteel tube) GC packed column is used.

2.2. Classical thermodynamics modelling

One of the objectives of this paper is to derive a thermodynamic model able to accurately correlate the VL equilibrium data acquired in this study. On account of its simplicity and accurateness, it was decided to use the Peng-Robinson equation of state with advanced mixing rules that combine the EoS with the residual part of an excess Helmholtz energy model, $a_{res}^{E,\gamma}$. For a mixture containing NC components with known mole fractions z_i, such mixing rules

write as follows [24, 25, 26]

$$\begin{cases} b_m = \sum_{i=1}^{NC}\sum_{j=1}^{NC} z_i z_j b_{ij}, \text{ with } b_{ij} = \left(\frac{b_i^{1/s} + b_j^{1/s}}{2}\right)^s \\ \frac{a_m}{b_m} = \sum_{i=1}^{NC} z_i \frac{a_i}{b_i} + \frac{a_{res}^{E,\gamma}}{\Lambda} \end{cases} \tag{1}$$

As a general rule, exponent s is set to a value lower or equal to 2. Parameter Λ is a constant, and its value depends on the selected cubic EoS. The pure-component parameters a_i and b_i are classically estimated from PR EoS by:

$$\begin{cases} X = \left[1 + \sqrt[3]{4-2\sqrt{2}} + \sqrt[3]{4+2\sqrt{2}}\right]^{-1} \approx 0.25308 \\ b_i = \Omega_b \frac{RT_{c,i}}{P_{c,i}}, \text{ with } \Omega_b = \frac{X}{X+3} \approx 0.077796 \\ a_i(T) = a_{c,i} \cdot \alpha_i(T), \text{ with:} \\ \quad a_{c,i} = \Omega_a \frac{R^2 T_{c,i}^2}{P_{c,i}}, \text{ and } \Omega_a = \frac{8(5X+1)}{49-37X} \approx 0.45723 \\ \quad \alpha_i(T) = \left[1 + \left(0.37464 + 1.54226\omega_i - 0.26992\omega_i^2\right)\left(1 - \sqrt{\frac{T}{T_{c,i}}}\right)\right]^2 \end{cases} \tag{2}$$

The Soave α-function incorporated in the original PR EoS model has been maintained as it retains a thermodynamically consistent behavior [27, 28, 29] in the whole temperature domain of interest for the two considered components (up to about 600 K for NO and 2000 K for SO_2). The PR EoS was not volume-translated [30, 31] since such a translation does not affect VL equilibrium calculations.

Following our previous studies on binary systems involved in CCS processes [16, 32], it was first decided to correlate the available data with the PPR78 model [33, 34]. For such a model, exponent s in equation (1) must be set to unity and the activity coefficient model ($a^{E,\gamma}$) is a one-parameter Van Laar expression:

$$\frac{a_{res}^{E,\gamma}}{\Lambda} = \frac{1}{2} \cdot \frac{\sum_{i=1}^{NC}\sum_{j=1}^{NC} z_i z_j b_i b_j E_{ij}(T)}{\sum_{i=1}^{NC} z_i b_i} \tag{3}$$

As required by equation (1), such an expression is a purely residual a^E model (it does not contain a combinatorial part). Following the mixing rule derived for the PPR78 model, the unique E_{12} parameter in equation (3) — needed to correlate the phase behavior of the NO + SO_2 binary system — was selected temperature-dependent through the following relation:

$$E_{12} = A_{12} \cdot \left(\frac{298.15}{T} \right)^{\left(\frac{B_{12}}{A_{12}} - 1 \right)}, \tag{4}$$

where A_{12} and B_{12} are two adjustable parameters. In order to improve the quality of the correlation, the Van Laar a^E model was subsequently replaced by the more sophisticated Wilson model. This second study was conducted because the NO + SO_2 mixture exhibits a type III phase behaviour and that such systems are known to be particularly difficult to correlate.

2.3. Molecular simulation techniques

The GIBBS Monte Carlo code [35] has been used to generate thermodynamic data for studied systems containing gaseous components and/or water and/or salts. VL equilibrium data were obtained with MC molecular simulations performed in the Gibbs NpT — isobaric-isothermal — ensemble where the number of particles (N), the total pressure (P) and the temperature (T) are constant [36, 37]. During these MC simulations, vapour and liquid phases are simultaneously considered in two distinct simulation boxes, without considering their interface. Transfers of particles between the two simulation boxes ensure the chemical equilibrium of the system. The sampling of the configurational space is ensured by different Monte Carlo moves, such as rigid body translations or rotations of molecules, and volume changes. The used MC moves and associated attempt probalities are as follows: rigid body translations (0.2975), rotations (0.2975), volume changes (0.0050), and transfers (0.4000). For translation, rotation, and volume change moves, maximum amplitudes were adapted to reach acceptance rates of 0.4. The studied systems contained in between 1000 and 2000 molecules depending on the vicinity of the critical point. For each MC

simulation, the number of generated configurations ranged within 2.10^8 and 2.10^9 including the equilibration of the system and the production run.

In the case of strongly associated systems such as brines, the above mentioned MC moves are not efficient enough to sample the configurational part of the phase space, and reaching the equilibrium state may necessitate important computational resources. To improve the sampling efficiency, we performed Hybrid Monte Carlo Molecular Dynamics (HMCMD) simulations [38, 39]. An HMCMD move consists in letting the system evolves deterministically through the phase space using a short Molecular Dynamics (MD) run as a MC move, in addition to other usual moves. In contrast to MC simulations, MD simulations enable the exploration of the whole phase space (*i.e.* all possible values of positions and momenta) with collective motions of all particles at each time step. MD steps were performed using the NEWTON Molecular Dynamics code developed for flexible and rigid molecules [40]. Hereafter, a HMCMD move corresponds to 50 MD steps with an adjustable MD time step so as to reach an average acceptance ratio of *ca.* 40%. All details regarding the implementation and the combination of the GIBBS and NEWTON codes are given elsewhere [39].

Molecular Dynamics simulations were performed with the NEWTON code to generate osmotic pressure values following the method proposed by Luo and Roux [41]. It consists in introducing virtual walls in the simulation box to separate brine and pure water regions, only water molecules can move from one region to the other. Forces resulting from interactions of ions with the walls are handled by a harmonic potential (with a constant of 41.9 kJ.mol^{-1}.Å^{-2}). The walls are placed with a separation distance in agreement with the desired ionic concentration. Ions leaving the constraint zone feel a force in the opposite direction (normal to the wall) in order to maintain them inside the ionic region (between the walls). The total average force exerted by the ions to the walls is directly related to the osmotic pressure. MD simulations start with an equilibration period where the system is relaxed by means of a 1 ns run using the NPzzT ensemble (Pzz = 0.1 MPa and T = 298.15 K), relaxing the size of the simulation box in the z direction. During this equilibration period, the

distance between walls is fixed in order to preserve the volume occupy by ions (i.e. the ionic concentration of the system). After this period the average box size in z direction is computed and the average Lz value is imposed to the system. Then, an additional 2 ns equilibrium simulation in the NVT ensemble (T = 298 K) is performed and followed by a 5 ns production run. Three different simulation runs, starting from independent initial configurations, were used to produce average values of the osmotic pressure for each system. The orthorhombic simulation boxes are composed of about 3000 water molecules divided into two regions: one contains the brine and the other contains pure water, with the pure water region representing two thirds along the z-axis.

2.4. Molecular models and force fields

As described hereafter, only rigid body molecules are considered thus no intramolecular energy has been computed. The total potential energy of the systems is calculated as the sum of the two contributions: dispersion-repulsion interactions (U_{disp} and U_{rep}) and the electrostatic energy (U_{elec}). A 12-6 Lennard-Jones (LJ) potential (equation (5)) has been used to represent the dispersion-repulsion energy between two force centres i and j belonging to different molecules and separated by a distance r_{ij}. During MC and MD simulations, U_{ij} interactions were evaluated using a spherical cut-off radius equal to half the size of the cubic simulation box, associated with standard long-range corrections.

$$U_{ij} = U_{rep} + U_{disp} = 4\epsilon_{ij}\left(\left(\frac{\sigma_{ij}}{r_{ij}}\right)^{12} - \left(\frac{\sigma_{ij}}{r_{ij}}\right)^{6}\right), \tag{5}$$

where ϵ_{ij} and σ_{ij} are the LJ parameters, and equations (6) and (7) present the Lorentz-Berthelot combining rules used to compute cross interaction parameters.

$$\epsilon_{ij} = \sqrt{\epsilon_i \epsilon_j}, \tag{6}$$

$$\sigma_{ij} = \frac{\sigma_i + \sigma_j}{2}. \tag{7}$$

During both MC and MD simulations, U_{elec} was computed from the Coulomb law (equation (8)) and evaluated using the Ewald summation method with 7 vectors in each direction of the space and a gaussian width set to $2\pi/L$, where L is the length of the cubic simulation box.

$$U_{elec} = \frac{1}{4\pi\epsilon_0}\frac{q_i q_j}{r_{ij}}, \tag{8}$$

where q_i and q_j are two point charges belonging to different molecules and spaced by r_{ij}, and ϵ_0 is the vacuum permittivity.

Values of ϵ_i, σ_i, and q_i parameters constitute the force field parameters. The GIBBS MC and the NEWTON MD simulation codes have both already been successfully used with intermolecular potentials listed in Table 2, and calculations have already shown good accuracy in the restitution of both equilibrium and/or transport properties for pure SO_2, NO, CO_2, N_2, and O_2 as well as some mixtures of these gases [6, 20, 21].

Force field parameters used to mimic SO_2, NO, CO_2, N_2, and O_2 are summarized in Table 2. The model developed by El Ahmar *et al.* has been used to mimic properties of sulphur dioxide [20]. The SO_2 molecule is represented as follows: each atom of the molecule is a LJ centre, and the S−O distance and the $\widehat{OSO}$ angle are equal to 1.434 Å and 119.50°, respectively. A negative point charge is located on each oxygen atoms, and q^+ a positive point charge is placed on the bisector of the $\widehat{OSO}$ angle at 0.312 Å from the sulphur atom, as illustrated in Table 2. The force field chosen to restitute molecular nitric oxide behavior was developed by Lachet *et al.* [21]. It consists of a single Lennard-Jones sphere. Note that this model well reproduces the variation of mole fraction of associated N_2O_2 as a function of temperature along the saturation line for the bulk liquid phase of the $2NO \rightleftharpoons N_2O_2$ system. The carbon dioxide has been extensively studied using molecular simulations, and the rigid version of the rescaled elementary physical model (EPM2) proposed by Harris and Yung [42] has shown that VL equilibrium data for pure CO_2 are well reproduced. Each atom carries both a LJ centres and an electrostatic point charge, and the C−O distance is

Table 2: Force field parameters for the studied molecules.

Molecule	Force centre or charge	σ(Å)	ϵ(K)	q(|e|)	Ref.
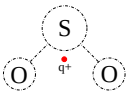	S	3.5830	126.0800	—	[20]
	O	2.9900	46.4100	-0.4140	
	q^+	—	—	0.8280	
	NO	3.4000	130.0000	—	[21]
	O	3.0330	80.5070	-0.3256	[42]
	C	2.7570	28.1290	0.6512	
	N	3.3000	36.0000	-0.5075	[43]
	q^+	—	—	1.0150	
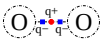	O	3.1062	43.1830	—	[44, 45]
	q^-	—	—	-2.1000	
	q^+	—	—	4.2000	
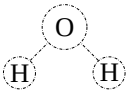	O	3.1655	78.1974	-0.8476	[46]
	H	—	—	0.4238	
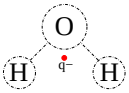	O	3.1589	93.1990	—	[47]
	H	—	—	0.5564	
	q^-	—	—	-1.1128	

equal to 1.149 Å. It is important to mention that although the model has been developed using geometric combining rules, Nieto-Draghi *et al.* have shown that the combination of the EPM2 force field parameters with the Lorentz-Berthelot rules allows a good restitution of both thermodynamic and transport properties [48]. The molecular nitrogen has been represented using the force field developed by Delhommelle [43]. The two N atoms are separated by 1.098 Å and each of them carries a LJ centre and a negative charge, a positive charge is placed on the centre of mass (CoM) of the molecule. On the basis of previous works, we have decided to mimic the oxygen behaviour using the Boutard *et al.* adaptation [45] of the Vrabec potential [44]. The two oxygen atoms carry each a LJ centre, and are separated by 1.210 Å. A positive electrostatic charge is located in between the two O atoms, and two negative charges are placed at 0.200 Å on both sides of the CoM of the molecule along the O−O bond.

Numerous potentials have been developed to mimic water properties with varied associated performances [49]. Among existing, we chose two widespread used models: the extended simple point charge (SPC/E) [46] and the transferable intermolecular potential with 4 sites (TIP4P/2005) [47], being aware of limitations of models involving rigid geometries and fixed electrostatic charges (*i.e.*, non-polarizable models) [50, 51]. In the two selected models water is considered as a rigid body molecule, the oxygen atom of the molecule is a LJ centre and hydrogen atoms carry positive charges. The $\widehat{\mathrm{HOH}}$ angle is 109.47° and 104.52° for the SPC/E and TIP4P/2005 models, respectively. For the SPC/E model, a negative point charge is placed on the oxygen atom and the O−H bond length is 1.000 Å. For the TIP4P/2005 model, a negative point charge is placed on the bisector of the $\widehat{\mathrm{HOH}}$ angle at 0.1546 Å from the oxygen atom, and the O−H bond length is 0.9572 Å. All details regarding force field parameters are summarized in Table 2. Sakamaki *et al.* compared performances of 12 non-polarizable water models including the SPC/E and TIP4P/2005 models to calculate, among others properties, VL equilibrium densities for temperatures from about 200 K to 650 K [52]. Recently, Vinš *et al.* performed a similar study focusing on the SPC/E and TIP4P/2005 models [53]. In this latter work, au-

Table 3: Force field parameters considered for the sodium and chloride ions: OPLS, Whee, GoS, GoT, and Aqv refer to the parameter set proposed by Jorgensen *et al.*, the parameter set proposed by Wheeler and Newman, the parameter set proposed by Goo *et al.* in combination with SPC/E, the parameter set proposed by Goo *et al.* in combination with TIP4P/2005, and the parameter set proposed by Åqvist, respectively.

Label	Ion	LJ centre		Ref.
		σ(Å)	ϵ(K)	
OPLS	Na^+	1.8974	808.7	[54, 55]
	Cl^-	4.4172	59.3	
Whee	Na^+	2.3500	55.3	[56]
	Cl^-	4.4200	54.2	
GoS	Na^+	2.5864	50.3	[57]
	Cl^-	4.4044	50.3	
GoT	Na^+	2.5931	42.2	
	Cl^-	4.4111	42.2	
Aqv	Na^+	3.3304	1.4	[54, 55, 58]
	Cl^-	4.4172	59.3	

thors reported the following absolute deviations from experimental data: (i) at 250 K, 0.6% and 0.2% for the SPC/E and TIP4P/2005 models, respectively (ii) and at 500 K, 5.3% and 1.9% for the SPC/E and TIP4P/2005 models, respectively. We performed similar simulations and our results agreed with previous observations.

We have considered five sets of parameters for the sodium (Na^+) and chloride (Cl^-) ions in which both of them are represented as a sole LJ sphere with an associated positive (+1|e|) charge and negative (-1|e|) charge, respectively. Force field parameters used to mimic the sodium (Na^+) and chloride (Cl^-) ions are summarized in Table 3. Neyt *et al.* have computed densities for NaCl aqueous solutions at 298 K and 0.1 MPa covering molalities up to 5.5 mol.kg^{-1}, and demonstrated that the combination OPLS with TIP4P/2005 performs better than others such as Reif [59] with TIP4P/2005 [60, 61]. Orozco *et al.* compared some salt models combined with SPC/E based water potentials for tempera-

Table 4: Force field parameters considered for the calcium and chloride ions: Matt, GoS, GoT, Pred, and Aqv refer to the parameter set proposed by Matthews *et al.* and Jorgensen *et al.*, the parameter set proposed by Goo *et al.* in combination with SPC/E, the parameter set proposed by Goo *et al.* in combination with TIP4P/2005, the parameter set proposed by Předota *et al.*, and the parameter set proposed by Åqvist, respectively.

Labels	Ions	LJ centre		Ref.
		σ(Å)	ϵ(K)	
Matt	Ca^{2+}	2.7101	15.1	[54, 55, 64]
	Cl^{-}	4.4172	59.3	
GoS	Ca^{2+}	1.5944	85.6	[57, 65]
	Cl^{-}	4.4044	50.3	
GoT	Ca^{2+}	1.6011	71.8	
	Cl^{-}	4.4111	42.2	
Pred	Ca^{2+}	2.8950	50.3	[66, 67]
	Cl^{-}	4.4010	50.3	
Aqv	Ca^{2+}	2.4120	226.3	[54, 55, 58]
	Cl^{-}	4.4172	59.3	

tures and pressures up to 473 K and 1000 bar, respectively [62].

Five sets of parameters have been considered to describe calcium (Ca^{2+}) and chloride (Cl^{-}) ions in which both of them are represented as a sole LJ sphere with an associated positive (+2|e|) charge and negative (-1|e|) charge, respectively. Force field parameters used to mimic the calcium (Ca^{2+}) and chloride (Cl^{-}) ions are summarized in Table 4. Note that Tsai *et al.* recently compared three sets of parameters including GoS and Aqv using two point charge based models (SPC and SPC/E) for water [63]. Performed comparisons have revealed that among the 6 considered combinaisons for water — $CaCl_2$ models, SPC/E — Aqv gives the best density predictions at 373 and 473 K with, nevertheless, a significant underestimation of experimental denisties at 373 and 473 K.

2.5. Electronic structure calculations

The electronic structure calculations were performed with the Gaussian 09 suite of programs [68]. All geometry optimizations were performed with the hy-

brid M06 functional [69] using the spin unrestricted formalism (uM06), in combination with the 6-311+G(d,p) basis set. Systematic conformational searches were performed to identify the most stable structures. Standard convergence criteria were applied, *i.e.* 1×10^{-8} Hartree for the electronic energy convergence, while for the geometry, convergences of 0.00045 and 0.00030 Hartree/Bohr for respectively the maximum and root mean square (RMS) forces were used, and threshold values of 0.0018 and 0.0012 Bohr for the maximum and RMS displacements, respectively. The character of the localized stationary points, *i.e.* minimum or first order transition state, on the potential energy surface was determined by calculating the Hessian matrix (2^{nd} derivative of the energy with respect to the atomic displacements). Furthermore, using intrinsic reaction coordinate (IRC) calculations it was verified that the transition state indeed connects reactants and products. Thermodynamic (enthalpic and entropic) contributions were calculated with the use of the partition functions within the harmonic oscillator and the perfect gaz approximation. Additionally, the resulting calculated vibrational frequencies have not been adjusted with an empirical correction factor. After the desired character of the stationary point was confirmed, the electronic wavefunction was subjected to a stability analysis to verify the presence of any singlet/triplet or doublet/quartet instabilities.

In this study, the uM06 functional in combination with the 6-311+G(d,p) basis set was selected, since it reproduces reasonably well the electronic state of the NO dimer. The NO dimer seems best described using a multi-reference method together with a large basis set [70], however, these methods can quickly become prohibitive for the systems investigated in this study, with respect to the needed computer resources.

3. Results and discussion

In this section, we present a series of new VL experimental data, together with modelling data obtained using both EoS and molecular simulation tools. We investigate NO + SO_2 systems using the three above mentioned techniques

(experimental, EoS, molecular simulations). Concerning molecular simulation we first studied chemical reactions that may occur in the gas phase and we then generate simulated vapour liquid equilibrium data for a broad range of temperatures. We then move our focus on the solubility of different gases (CO_2 and associated gases such as O_2, N_2, SO_x, NO_x) in brines. For this second study, simulation results are divided into two main parts devoted to the study of the solubility in water and in brines, respectively. The solubility is first expressed in terms of Henry constant values. In the case of sulphur dioxide solubility in water, we characterize deviations to the Henry's law with increasing pressure conditions. A similar solubility study is then proposed in the case of brines containing NaCl or $CaCl_2$. We present a comparison of some combinations of salt and water potentials in terms of density and osmotic pressure predictions. We propose the generation of simulated Henry constant values for CO_2, SO_2, NO, O_2, and N_2 in brines considering various salt concentrations and temperatures.

3.1. Investigation of chemical reactions within NO + SO_2 systems

Before studying phase equilibrium in NO + SO_2 systems, we first investigate the stability of such mixtures by means of electronic structure calculations. Such calculations have been performed in the gas phase, considering the following chemical reaction: SO_2 + 2 NO $\rightleftharpoons$ SO_3 + N_2O. With the use of the applied method (see section 2.5) the singlet spin $^1A_1$ is calculated to be slightly more stable than the $^3B_2$ triplet state by 0.99 kcal.mol^{-1}, which is in accordance with the CASSCF results of Sayos *et al.* [71], see Table 5. However, it appears that the calculated singlet electronic structure has an instability, while the triplet state is stable under the considered perturbations. We therefore have taken the triplet state as the most stable electronic configuration. All other calculated species have a singlet electronic ground state, except for NO, where the doublet spin state is largely more stable than the quartet spin state (>123 kcal.mol^{-1}).

The here applied method correctly reproduces the dimer dissociation energy (probably as a result of a fortunate cancellation of errors). Yet, the bond distances are slightly less well reproduced. Since we are mostly interested in the

energetics in this study, we consider this of smaller importance.

Figure 1 shows the energy reaction profile for the SO_2 + 2 NO reaction to yield SO_3 and N_2O for the electronic energy corrected for the zero-point energies (ZPE), the enthalpy changes at 298 K and the Gibbs energy at 298 K and 0.1 MPa. Starting with the reactants, 2 NO and SO_2 (**M0**), first the *cis* NO dimer is formed with the SO_2 molecule at infinite distance (**M1**). Then the system goes through a transition state, where one NO molecule is nearly 90 degrees rotated and the $\widehat{\text{ONNO}}$ dihedral angle changes from 0.0 in M1 to -84.3 degrees in **T1**. Next, the NO molecule continues its rotation to obtain a geometry where the two NO molecules are again in the same plane (**M2**). However, this configuration now more corresponds to the *trans* dimer, where one of the two molecules is shifted. Next, the transition takes place in which an oxygen atom is transferred from one NO molecule to the SO_2 molecule. This transition state (**T2**) is characterized by an imaginary frequency of $i745.1$ cm^{-1} and a NO distance of 1.433 Å in **T1** (1.147 Å in **M2**).

The very small energy barrier for the **M1** $\rightleftharpoons$ **T1** $\rightleftharpoons$ **M2** transition indicates a rapid *cis*/*trans* isomerization, while the significantly larger energy barrier for the **M2** $\rightleftharpoons$ **T2** $\rightleftharpoons$ **M3** transition corresponds to the rate determining step of the overall reaction.

Upon considering the three energy profiles in Figure 1 it is seen that all three clearly show that the overall reaction is thermodynamically favored. The thermal corrections (T = 0 K to T = 298 K) only have a minor impact on the relative stabilities of the different species, whereas the entropy significantly destabilizes both the transition state **T2** and the final products **M3**. As can be seen from Figure 2, the entropy (or more precisely the TΔS term) becomes smaller during the course of the reaction with an overall minimum for **T2**, where the three reactants essentially form one single species. An increase of the temperature, *e.g.* from 273 to 345 K, has an endergonic contribution to the Gibbs energy, while a pressure increase from 0.1 to 5.0 MPa yields an exergonic contribution to ΔG.

From Table 6 it is seen that the reaction barrier (ΔG_a) that corresponds to

Table 5: Properties of the *cis* NO dimer calculated at the M06 level, using the multi-reference CASSCF method [71], and experimental data. BE, ZPE, and E_{elec} stands for bonding energy, zero-point energy, and electronic energy, respectively.

	M06/ 6-311+G(d,p)	CASSCF(18,14)/ 6-311G(2d)	Exp.
BE (kcal.mol^{-1})	3.27	4.31	2.18 [72]
BE + ΔZPE (kcal.mol^{-1})	1.86	1.43	—
ΔE (kcal.mol^{-1})*	0.99	5.56	—
r(NN) (Å)	1.972	2.327	2.263 [73]
r(NO) (Å)	1.146	1.159	1.152 [73]

* $\Delta E = E_{elec}(\text{triplet, } {}^3B_2) - E_{elec}(\text{singlet, } {}^1A_1)$.

Table 6: Energy changes (kcal.mol^{-1}) of the most important transitions under different temperature and pressure conditions.

	ΔE+ΔZPE (0 K)	ΔH (298 K)	ΔG (298 K, 0.1MPa)	ΔG (298 K, 5MPa)	ΔG (345 K, 0.1MPa)
M0 ⇌ **M1**	-1.9	-2.6	5.9	3.6	7.2
M1 ⇌ **T1**	1.3	1.7	-0.2	-0.2	-0.4
M1 ⇌ **M2**	1.2	1.2	1.1	1.1	1.1
M2 ⇌ **T2** (Δ_a)	33.7	32.4	46.9	44.6	49.2
M0 ⇌ **M2** (Δ_R)	-39.8	-41.3	-29.0	-31.4	-27.1

the rate determining step (**M2** ⇌ **T2**), stays well beyond +40 kcal.mol^{-1} in the investigated temperature and pressure ranges. It can thus be concluded that, in spite of the fact the reaction is thermodynamically favored (ΔG_R), the overall reaction is kinetically prohibited. No chemical reaction will thus be considered hereafter in the study of NO + SO_2 systems.

3.2. VL equilibrium for NO + SO_2 systems

In this section, we propose new experimental VL data (generated using the apparatus described in section 2.1) for pressures up to 10 MPa. Molecular simulation tools were then used to supplement VL data at higher pressures.

Finally, all VL data were used to optimize settings of the PPR78 EoS.

The apparatus described above has been used to acquire experimental data for NO + SO_2 binary mixtures. In this work, only vapour phases have been sampled. Experimental vapour phase compositions have been measured for the NO + SO_2 binary mixtures at 273.07 K, 313.21 K, and 343.28 K, and pressures up to 10 MPa. So-obtained mole fractions are reported in Table 7. Figure 3 plots pressures against experimental NO mole fractions for vapour phases of the studied systems. New experimental data are compared with those reported by Xu *et al.* [16], and both sets are consistent.

VL equilibrium data were obtained using MC molecular simulations performed in the Gibbs NpT ensemble. The studied systems contained in between 1000 and 2000 molecules depending on the vicinity of the critical point of the studied mixture. For each MC simulation, the number of generated configurations ranged within 2.10^8 and 6.10^8 including the equilibration of the system and the production run. Statistical uncertainties associated to calculated phase properties were determined using the block averaging technique [74], and on liquid densities they are typically 1-2%, but higher values are found at near-critical temperatures as a result of larger fluctuations. Table 8 summarizes the calculated VL equilibrium data. Figure 3 presents pressure plotted against liquid and vapour phases mole fractions of NO, at 273.15, 293.15, 313.15, 324.15, and 345.15 K. The considered temperatures are below the SO_2 critical temperature (430.75 K), all phase diagrams exhibit a critical point, except that obtained at 273.15 K for which molecular simulations do not indicate an obvious closing trend of the phase envelope. Simulated critical coordinates of NO + SO_2 mixtures were estimated by extrapolating MC simulation results with scaling laws, as described in equations (9) and (10), and detailed in previous works [6, 19, 20, 35]. The so-obtained critical coordinates, *i.e.* the critical density ρ_c, the critical composition x_c, and the critical pressure P_c, are given in

Table 7: Experimental compositions of the vapour phase for NO + SO_2 binary mixtures at 273.07 K, 313.21 K, and 343.28 K. n is the number of samples, y_{NO} is the NO molar fraction in the vapour phase, and $\sigma_{y_{NO}}$ is the repeatability on vapour compositions. Umax(y) is 0.004, U(P) is 6.10^{-4} MPa, and U(T) is 0.02 K

P (MPa)	n	y_{NO}	$\sigma_{y_{NO}}$
	$T = 273.07$ K		
0.4866	6	0.6580	0.0020
1.0115	16	0.8283	0.0005
2.0609	11	0.9096	0.0002
3.2926	8	0.9372	0.0001
6.1645	6	0.9551	0.0002
10.8416	5	0.9618	0.0001
	$T = 313.21$ K		
1.2488	9	0.4390	0.0030
1.8063	8	0.6090	0.0020
3.2242	6	0.7570	0.0050
5.1040	5	0.8270	0.0040
9.2503	10	0.8580	0.0020
14.173	6	0.8810	0.0010
	$T = 343.28$ K		
2.2584	5	0.3091	0.0060
3.5153	6	0.5190	0.0040
5.5226	7	0.6530	0.0060
7.7624	7	0.7190	0.0040
9.9743	6	0.7420	0.0090
12.7731	6	0.7530	0.0040
16.1085	4	0.7620	0.0030

Table 8.

$$\rho_i = \rho_c + \zeta\frac{\gamma}{2}(P_c - P)^{\beta} + \lambda(P_c - P), \tag{9}$$

$$x_i = x_c + \left(\lambda_1 - \zeta\frac{\lambda_2}{2}\right)(P_c - P) - \zeta\frac{\mu}{2}(P_c - P)^{\beta}, \tag{10}$$

where, $\beta = 0.325$, and $\zeta = 1$ or -1 whether it refers to the liquid or vapour phase, respectively. Parameters (γ, λ, λ_1, λ_2, and μ) of equations (9) and (10) are regressed from a set of simulated coexistence data (*i.e.*, (P, ρ_l, ρ_v) and (P, x_l^{NO}, x_v^{NO}), where subscripts l and v denote the liquid phase and the vapour phase, respectively). Figure 4 presents pressure plotted against liquid and vapour phase densities at 273.15, 293.15, 313.15, 324.15, and 345.15 K. To the best of our knowledge, there is no volumetric data available in the literature to compare our results with.

Correlation of the NO + SO_2 binary system by means of the PPR78 EoS [16] was performed by Xu *et al.* who proposed to use $A_{12} = 172.3$ MPa and $B_{12} = 1343.2$ MPa, see equation (4). Such parameters were however determined considering only six experimental data points. In this study, it was decided to refit such parameters over all the available VL equilibrium data. The following objective function ($O.F.$) was minimized:

$$O.F. = \sum_{i=1}^{n.b.} |x_i^{exp} - x_i^{calc}(T_i^{exp}, P_i^{exp})| + \sum_{i=1}^{n.d.} |y_i^{exp} - y_i^{calc}(T_i^{exp}, P_i^{exp})| \tag{11}$$

where, $n.b.$ and $n.d.$ designate the number of bubble and dew points, respectively. The derived optimal parameters for equation (4) — not so different from the ones obtained by Xu *et al.* [16] —, are $A_{12} = 127.6$ MPa and $B_{12} = 856.8$ MPa. Figures 3 shows data points and results of calculation obtained with the PPR78 EoS model. Isothermal phase diagrams at T = 273.15 K, T = 293.15 K, T = 313.15 K, T = 324.15 K, T = 345.15 K (Figure 3) and the global phase equilibrium diagram for the NO + SO_2 mixture (Figure 5) were calculated.

Table 8: Calculated vapour liquid equilibrium compositions and densities for the NO + SO_2 mixture at different temperatures.

T (K)	P (MPa)	x_v^{NO}	ρ_v (kg.m^{-3})	x_l^{NO}	ρ_l (kg.m^{-3})	T (K)	P (MPa)	x_v^{NO}	ρ_v (kg.m^{-3})	x_l^{NO}	ρ_l (kg.m^{-3})
273.15	0.2#	0.00000	4.6	0.00000	1440.1	313.15	0.7#	0.00000	18.7	0.00000	1332.6
	1.5	0.01142	23.4	0.87258	1435.3		1.5	0.00808	28.6	0.52200	1325.5
	3.0	0.02517	44.9	0.93108	1425.8		3.0	0.02238	48.2	0.73322	1318.2
	5.0	0.04194	75.2	0.95070	1417.4		5.0	0.04151	75.1	0.82048	1307.1
	10.0	0.07994	158.2	0.96230	1399.4		10.0	0.08840	147.2	0.87900	1281.2
	15.0	0.11936	248.3	0.96373	1378.1		15.0	0.13611	224.9	0.88985	1252.3
	20.0	0.14771	342.8	0.95719	1366.1		20.0	0.18079	307.9	0.88492	1226.7
	25.0	0.17037	430.5	0.94785	1358.5		25.0	0.22725	391.8	0.87307	1198.5
	30.0	0.19672	502.8	0.93996	1346.1		30.0	0.27163	477.7	0.85127	1171.6
	35.0	0.22173	561.0	0.93484	1334.9		35.0	0.30865	569.8	0.81457	1152.1
	40.0	0.23590	615.2	0.92370	1332.8		40.0	0.38648	665.2	0.76935	1089.9
	45.0	0.26086	657.5	0.91681	1321.4		42.7*	0.56971	907.9	0.56971	907.9
	50.0	0.28289	691.2	0.91214	1312.0	324.15	0.9#	0.00000	24.6	0.00000	1297.1
	55.0	0.30074	725.5	0.90456	1306.8		3.2	0.02213	54.4	0.65618	1286.2
	60.0	0.31492	751.9	0.90049	1304.0		5.0	0.03982	78.1	0.75245	1275.8
	65.0	0.32828	784.4	0.88859	1302.1		10.0	0.08817	149.6	0.83536	1247.6
293.15	0.3#	0.00000	9.5	0.00000	1384.9		15.0	0.13662	225.5	0.85384	1218.9
	1.5	0.01046	25.0	0.73761	1381.8		20.0	0.19058	306.6	0.85384	1183.0
	3.0	0.02371	45.3	0.85498	1375.5		25.0	0.24291	398.8	0.83357	1147.6
	5.0	0.04170	73.6	0.90118	1366.4		30.0	0.30027	490.6	0.80785	1108.1
	10.0	0.08582	149.5	0.93121	1340.9		35.0	0.37495	595.1	0.76037	1047.0
	15.0	0.12644	232.1	0.93359	1319.7		37.8*	0.57676	836.2	0.57676	836.2
	20.0	0.16297	318.6	0.92786	1300.8	345.15	1.6#	0.00000	42.1	0.00000	1232.3
	25.0	0.20117	401.6	0.91891	1279.2		3.9	0.02411	73.9	0.50703	1223.6
	30.0	0.24074	478.7	0.90658	1256.3		7.0	0.05746	113.9	0.68165	1197.1
	35.0	0.27427	544.2	0.89477	1238.9		10.0	0.09115	156.6	0.74079	1173.3
	40.0	0.30313	602.5	0.88039	1225.0		15.0	0.15237	231.7	0.77920	1128.3
	45.0	0.33635	660.4	0.86152	1208.3		20.0	0.21368	318.0	0.77616	1086.2
	50.0	0.36514	716.1	0.83725	1194.2		25.0	0.28384	420.9	0.74666	1033.5
	55.0	0.41668	819.3	0.76114	1159.0		27.0	0.31836	456.2	0.73929	1001.0
	57.7*	0.58231	1007.4	0.58231	1007.4		29.0	0.36071	508.8	0.71747	960.8
							31.3*	0.54987	744.1	0.54987	744.1

* Critical coordinates obtained using extended scaling laws, see equations (9) and (10).

Pure SO_2 liquid vapour equilibrium data obtained using GIBBS NVT MC simulations.

As shown by Figure 5, the NO + SO_2 mixture exhibits a type III phase behaviour according to the classification scheme by van Konynenburg and Scott [75, 76]. The VL equilibrium data of such systems are acknowledged to be difficult to correlate with an EoS, and it is thus not surprising to observe deviations between calculated and experimental data points. In particular, the use of a one-parameter a^E model, like the van Laar model, in the advanced mixing rules implemented in this study tends to strongly overestimate critical pressures predicted using MC simulations. From our experience [24, 25, 26], the quality of the correlation can however be significantly improved by coupling the PR EoS with the residual part of the Wilson a^E model. For a binary system, such a model writes as follows:

$$\begin{aligned}\frac{a_{res}^{\gamma Wilson}(T,\zeta)}{RT} = &-z_1 \ln\left[\Phi_1 + \Phi_2 \exp\left(-\frac{A_{12}}{RT}\right)\right] \\ &-z_2 \ln\left[\Phi_1 \exp\left(-\frac{A_{21}}{RT}\right) + \Phi_2\right]\end{aligned} \tag{12}$$

A_{12} and A_{21} are the two adjustable parameters and $\Phi_i = z_i \mathbf{v}_i / \sum_{j=1}^{NC}(z_j \mathbf{v}_j)$ is the volume fraction of molecule i. Such an activity coefficient model was used in conjunction with equation (1) after setting parameter s to 2 and parameter Λ to -0.52398 (this is the value proposed by Michelsen during the derivation of the modified Huron-Vidal mixing rule [77]). As was done previously with the PPR78 EoS model, the objective function defined by equation (11) was minimized. The optimal parameters, determined for each isothermal group of data, are reported in Table 9. Both A_{NO-SO_2} and A_{SO_2-NO} vary according to the temperature, and the application of a curve fitting leads to polynomial functions of degree two allowing temperature interpolations.

Figure 3 shows data points and results of calculations obtained after coupling the PR EoS with the two-parameter $a_{res}^{\gamma Wilson}$ model (dashed lines). Such a figure clearly demonstrates that the correlation of both the critical regions and the dew curves have been highly improved as compared to PR with one-parameter a^E model (solid lines).

Table 9: Parameters A_{12} and A_{21} of the Wilson a^E model to use with the advanced mixing rules employed in this study.

T(K)	273.15	293.15	313.15	324.15	345.15
A_{NO-SO_2}	180	238	423	603	830
A_{SO_2-NO}	180	-57	-299	-420	-533

3.3. Henry constants of gases in water

The Henry constant (K_H) provides information about interactions between the solute and the solvent. At T and P conditions, the Henry constant for a solute i (*i.e.* gas, in this work) in a solvent (*i.e.* water or brines, in this work) is defined as follows:

$$K_H(\mathrm{T,P}) = \lim_{x_i \to 0} \frac{f_i}{x_i}, \tag{13}$$

where f_i and x_i are the fugacity and the mole fraction of the solute i, respectively. f_i is related to the excess chemical potential ($\overline{\mu}_i(\mathrm{T,P},x_i)$) by:

$$\frac{f_i}{x_i} = \mathrm{P}exp(\beta\overline{\mu}_i(\mathrm{T,P},x_i)), \tag{14}$$

where $\beta = 1/k_\mathrm{b}T$ and k_b is the Boltzmann's constant. Solubilities of gases in a solvent have been computed using the Widom test insertion technique which consists in randomly inserting a particle in the solvent. The difference in potential energy (ΔU^+) resulting from the particle insertion in the solvent is calculated, and the excess chemical potential at infinite dilution is evaluated using equation (15).

$$\overline{\mu}_i(\mathrm{T,P},x_i) = -\frac{1}{\beta}\ln\left\langle \frac{\beta PV}{N+1}\exp\big(-\beta\Delta U^+\big)\right\rangle_{NpT}, \tag{15}$$

with V the volume of the system, see reference [78] for more details.

We performed MC simulations in the NpT ensemble for SO_2/H_2O, NO/H_2O systems, and for three other systems: CO_2/H_2O, O_2/H_2O, and N_2/H_2O, in order to obtain Henry constant values. Temperatures ranged from 273.15 K to

623.15 K, and the pressure was set to the corresponding vapour pressure, P^{sat}, of water. Simulation boxes contained 10^3 water molecules represented with the TIP4P/2005 potential, as this latter is known to better reproduce liquid densities as compared to the SPC/E potential [52, 53]. Note that no finite size effect has been detected by Orozco *et al.* using simulation boxes with 300 water molecules [79]. Gas molecules were described using force fields listed in Table 2. For each system, 5×10^8 MC configurations were generated and K_H evaluated using equations (14) and (15). The statistical uncertainty associated to simulated K_H value is 20%, determined using the block averaging technique [74]. Lísal *et al.* have generated K_H values for CO_2 using MC simulations together with SPC based water potentials and three potentials including the EPM2 to mimic CO_2 behavior, and authors showed that the combination SPC/E – EPM2 qualitatively predicts the temperature dependence of the Henry constant [78]. This latter combination fails in reproducing the maximum in K_H experimentally observed at *ca.* 420 K which corresponds to the temperature at which the enthalpy of solution is zero [78, 80]. More recently, Orozco *et al.* showed that K_H values obtained with TIP4P/2005 – EPM2 are lower than predictions using SPC/E – EPM2 [79]. Simultaion results reported in Table 10 supplement these latter data with K_H values for temperatures up to 623.15 K, using the TIP4P/2005 – EPM2 model. The simulated maximum in K_H is observed at *ca.* 450 K, but simulation results overestimate experimental K_H values. Molecular simulations were also performed to obtain K_H values for SO_2, NO, O_2, and N_2 in water for temperatures ranging from 273.15 K to 623.15 K, see Table 10. Figure 6 illustrates K_H evolutions as a function of the temperature, for gases of interest. Beside NO, molecular simulation results reasonably agree with correlations of experimental values [81, 82], and the temperature value at which the enthalpy of solution is zero – the maximum in K_H – is well estimated.

3.4. Solubility of sulphur dioxide in pure water

In the case of sulphur dioxide (gas with the lowest K_H values in Table 10), we propose to supplement the information (Henry constant values) provided in

Table 10: Simulated Henry constants for SO_2, CO_2, NO, O_2, and N_2 in water for temperatures ranging from 273.15 K to 623.15 K.

Temperature (K)	Henry constant (MPa.mol/mol)				
	SO_2	CO_2	NO	O_2	N_2
273.15	3	174	1826	2308	6172
323.15	36	510	4838	6333	15683
373.15	70	885	6150	6871	14354
423.15	104	934	5061	5252	9522
473.15	134	976	3447	3806	6167
523.15	150	808	2185	2354	3405
573.15	138	564	1252	1390	1836
623.15	120	360	671	708	854

Table 10 by computing SO_2 solubility in water at higher pressure values beyond the Henry regime. At the two investigated temperatures (298.15 K and 323.15 K), phase diagrams for the SO_2 + H_2O binary mixtures exhibit a liquid vapour (L1,V) equilibrium domain at the lowest pressures, a liquid-liquid (L1,L2) equilibrium domain at the highest pressures, with a three-phase line (L1,L2,V) in between these two domains, and a tiny liquid vapour (L2,V) domain just above the three-phase line near the pure SO_2 axis. MC molecular simulations were performed in the Gibbs ensemble for pressures up to 10 MPa, in the Gibbs-NpT ensemble for diphasic systems and in the Gibbs-NVT ensemble for triphasic systems. The studied systems contained in between 550 and 1000 molecules. For each MC simulation, the number of generated configurations ranged within 2.10^8 and 4.10^8 including the equilibration of the system and the production run. Table 11 presents simulated phase compositions for the SO_2 + H_2O systems, and Figure 7 proposes comparisons with available experimental data, for the H_2O-rich part of the pressure-composition diagram. Table 11 contains information regarding coordinates of the three-phase line in between the vapour-liquid and the liquid-liquid equilibrium domains, located at 0.41 MPa and 0.86 MPa at 298.15 K and 323.15 K, respectively. Comparisons with available experimen-

tal data performed in Figure 7 indicate that the SO_2 content of the water-rich branch of the liquid-liquid domain is slightly underestimated by molecular simulations. Using solubility data presented in Table 11, one can estimate Henry constant values: 9 MPa.mol/mol at 298.15 K and 33 MPa.mol/mol at 323.15 K, in line with values reported in Table 10.

3.5. Liquid densities and osmotic pressures for brines

For binary H_2O/NaCl and H_2O/$CaCl_2$ systems, we propose to supplement the information available in the litterature regarding the prediction of brine liquid density values using non-polarizable intermolecular potentials. Thus, we performed HMCMD simulations in the NpT ensemble for NaCl or $CaCl_2$ aqueous solutions with molalities from 0 to 5 mol.kg^{-1}, at 298 K and 0.1 MPa. Our simulation boxes contain 500 water molecules and up to 45 salt molecules (NaCl or $CaCl_2$). We did not investigate size effects but Tsai *et al.*, who considered similar binary systems with smaller simulation box size, have reported no or negligible finite-size effects [63].

Table 12 details obtained simulated density values for NaCl aqueous solutions at 298 K and 0.1 MPa. Figure 8 presents the simulated density values as a function of brine molal concentrations for each of the considered couple water − NaCl models. Predictions obtained with all combinations follow the experimental trend, *i.e.* the binary system density increases with the salt molality. Among the tested combinaisons, TIP4P/2005 − OPLS leads to the most accurate predictions with respect to experimental data proposed by Zhang and Han [83], with a MAE of 2.5 kg.m^{-3}. The use of the SPC/E − OPLS combinaison leads to a similar predictive accuracy with a MAE of 2.6 kg.m^{-3}. Although the Wheeler potential has been designed using the SPC/E model, its combination with the TIP4P/2005 water model results in satisfactory predictions with a MAE of 4.0 kg.m^{-3}. The use of other tested combinations significantly underestimates density values for all investigated salt molalities. The osmotic pressure is an interesting thermodynamic property to evaluate the accuracy of force fields for concentrated aqueous salt solutions. MD simulations were per-

Table 11: Phase compositions for the SO_2 + H_2O binary systems at 298.15 K and 323.15 K, obtained using MC molecular simulation. V denotes the vapour phase, and L1 and L2 stand for H_2O-rich and SO_2-rich liquids, respectively. Water molecules are mimicked using the TIP4P/2005 potential.

P	Molar fraction of SO_2		
(MPa)	L1	L2	V
	T = 298.15 K		
0.05	0.00429	—	0.98663
0.10	0.01071	—	0.99304
0.41	0.04427	0.99020	0.99833
0.42	—	1.00000	1.00000
0.50	0.04040	0.98755	—
1.00	0.04124	0.98879	—
3.00	0.04143	0.98819	—
5.00	0.04254	0.99163	—
10.00	0.04229	0.97244	—
	T = 323.15 K		
0.05	0.00165	—	0.93193
0.10	0.00397	—	0.96244
0.50	0.01547	—	0.99275
0.86	0.04312	0.98178	0.99588
0.91	—	1.00000	1.00000
1.00	0.03925	0.98104	—
3.00	0.04412	0.97657	—
5.00	0.03935	0.97821	—
10.00	0.03444	0.97999	—

formed for the TIP4P/2005 – OPLS and the SPC/E – OPLS combinations, considering four salt molal concentrations (m from 1.0 to 4.5 mol.kg^{-1}), at 298 K. Table 14 presents simulation results, and Figure 9(A) proposes a comparison of predicted values with experimental data extracted from reference [84]. The comparison shows that osmotic pressure values obtained with the TIP4P/2005 – OPLS combination are in better agreement with respect to reference experimental data (MAE = 0.4 MPa) as compared to osmotic pressures calculated with the SPC/E – OPLS combination (MAE = 1.5 MPa). Consequently, the TIP4P/2005 – OPLS will be the only combination considered hereafter for binary H_2O/NaCl systems.

Table 13 summarizes density values for aqueous $CaCl_2$ solutions, using HMCMD simulations at 298 K and 0.1 MPa. Figure 8 presents the simulated density values as a function of brine molal concentrations for each of the considered couple water – $CaCl_2$ models. Results show that the best density predictions are obtained using the potential developed by Goo *et al.* and the TIP4P/2005 water models, with a MAE of 7.6 kg.m^{-3}. Tsai *et al.* recently studied $CaCl_2$ aqueous solutions by means of molecular simulations and only SPC based water models, and concluded that the SPC/E – Aqv outperforms all other tested combinations. From comparisons performed in Figure 8, we demonstrate that when using SPC/E water model, more accurate density predictions can be obtained with the potential developed by Goo *et al.*, with a MAE of 9.6 kg.m^{-3}. Then, MD simulations were performed using the TIP4P/2005 – GoT and the SPC/E – GoS combinations, and simulation conditions similar to those performed in the case of NaCl aqueous solutions in order to investigate osmotic pressures. Table 14 presents simulation results, and Figure 9(B) proposes a comparison of predicted values with experimental data extracted from the work of Staples and Nuttall [85]. Comparisons show that none of the two investigated combinations successfully reproduces experimental osmotic pressure values, with MAE greater than 20 MPa. Hereafter, the TIP4P/2005 – GoT model will be used to mimic the behavior of $CaCl_2$ aqueous solutions.

Table 12: Simulated liquid density values for aqueous NaCl solutions varying the salt molal concentration from 0 to 5 mol.kg^{-1}, at 298 K and 0.1 MPa, obtained using HMCMD simulations in the NpT ensemble and force fields listed in Table 3.

Water − NaCl models	m (mol.kg^{-1})	Density (kg.m^{-3})	Water − NaCl models	m (mol.kg^{-1})	Density (kg.m^{-3})
TIP4P/2005	0	997.6	TIP4P/2005 − Whee	1	1038.2
TIP4P/2005 − OPLS	1	1038.9		2	1071.9
	2	1074.8		3	1102.3
	3	1110.1		4	1129.8
	4	1140.3		5	1157.2
	5	1164.5	SPC/E	0	999.0
TIP4P/2005 − GoT	1	1036.4	SPC/E − OPLS	1	1035.6
	2	1069.7		2	1071.5
	3	1098.4		3	1106.6
	4	1126.4		4	1132.9
	5	1148.0		5	1159.1
TIP4P/2005 − Aqv	1	1030.1	SPC/E − GoS	1	1032.7
	2	1060.7		2	1060.5
	3	1082.1		3	1088.6
	4	1105.6		4	1116.8
	5	1123.9		5	1136.2

Table 13: Simulated liquid density values for aqueous $CaCl_2$ solutions varying the salt molal concentration from 0 to 5 mol.kg^{-1}, at 298 K and 0.1 MPa, obtained using HMCMD simulations in the NpT ensemble and force fields listed in Table 4.

Water − $CaCl_2$ models	m (mol.kg^{-1})	Density (kg.m^{-3})	Water − $CaCl_2$ models	m (mol.kg^{-1})	Density (kg.m^{-3})
TIP4P/2005	0	997.6	SPC/E	0	999.0
TIP4P/2005 − Aqv	1	1078.0	SPC/E − GoS	1	1083.3
	2	1143.7		2	1152.6
	3	1196.1		3	1217.9
	4	1232.4		4	1273.4
	5	1264.3		5	1315.6
TIP4P/2005 − Matt	1	1061.3	SPC/E − Pred	1	1077.2
	2	1108.1		2	1135.2
	3	1156.9		3	1186.8
	4	1194.2		4	1218.4
	5	1231.2		5	1252.7
TIP4P/2005 − GoT	1	1082.4	SPC/E − Aqv	1	1077.1
	2	1152.6		2	1137.9
	3	1218.7		3	1193.2
	4	1273.5		4	1225.7
	5	1326.5		5	1266.6

Table 14: Osmotic pressure values (MPa) for aqueous NaCl and $CaCl_2$ solutions varying the salt molal concentration from 1 to 5 mol.kg^{-1}, at 298 K and 0.1 MPa, obtained using MD simulations in the NVT ensemble and force fields listed in Tables 3 and 4.

NaCl				$CaCl_2$			
m	TIP4P/2005 − OPLS	m	SPC/E − OPLS	m	TIP4P/2005 − GoT	m	SPC/E − GoS
1.04	4.22	1.03	4.82	1.0	4.82	1.0	6.98
2.19	10.27	2.10	9.34	2.3	13.56	2.3	17.00
3.51	18.73	3.33	19.04	3.6	22.67	3.6	30.59
4.49	24.36	4.48	27.78	4.9	38.51	4.9	49.07

3.6. Henry constants of gases in brines

We performed MC simulations in the NpT ensemble to compute Henry constant values for SO_2, CO_2, NO, O_2, and N_2 in brines. Investigated temperatures ranged from 298.15 K to 373.15 K, and the pressure was set to the corresponding vapour pressure of the brine which is assumed similar to that of water in the range of investigated salt concentrations. From conclusions drawn in previous sections, simulation boxes contained 10^3 water molecules represented with the TIP4P/2005 potential, and NaCl and $CaCl_2$ mimicked using the OPLS (see Table 3) and GoT (see Table 4) parameterizations, respectively. Gas molecules were described using force fields listed in Table 2. Up to 2×10^9 MC configurations were generated for each system, and K_H evaluated according to equations (13) to (15). The mole fraction of the solute (gas molecule inserted in the simulation box) is defined as 1/(N+1), with N the number of solvent species in the simulation box. In the case of brines, N can be estimated either considering anions and cations coupled or not; salt ions are supposed uncoupled hereafter. Due to the low acceptance of insertions for high salt concentrations and resulting problems of statistics, we chose to limit the present study to brines with salt molalities up to 3 mol.kg^{-1}. Tables 15 and 16 report simulated Henry constant values for NaCl and $CaCl_2$ aqueous solutions, respectively. Figure 10 illustrates K_H values simulated for gases in NaCl aqueous solutions. The statistical uncertainty associated to simulated K_H value is 20%, determined using the block averaging technique [74]. Our proposed sets of simulated Henry constant values can be used to estimate Sechenov constant (K_S) values as defined in equation (16) [86, 87].

$$\log\left(\frac{K_H^b}{K_H^w}\right) = K_S.m, \tag{16}$$

where m is the salt molality, and K_H^w and K_H^b denotes Henry constants in water and brine, respectively. For studied temperatures and NaCl brines, K_S values for CO_2, NO, O_2, and N_2 in NaCl aqueous solutions lie in between 0.11 and 0.15 kg.mol^{-1}, and K_S values for SO_2 range from 0.07 to 0.22 kg.mol^{-1}. In the

Table 15: Simulated Henry constants for some gases in NaCl aqueous solutions for temperatures ranging from 298.15 K to 373.15 K.

Temperature	m	Henry constant (MPa.mol/mol)				
(K)	(mol.kg^{-1})	SO_2	CO_2	NO	O_2	N_2
298.15	1	20	548	6225	7288	18861
	2	39	744	10273	11813	33861
	3	55	909	12209	14389	38511
323.15	1	48	845	8222	9362	23340
	2	64	1318	11935	13672	36873
	3	84	1295	13945	15868	41267
373.15	1	87	1298	8683	9675	21086
	2	102	1734	11747	13177	29267
	3	111	2248	15739	17627	39944

case of $CaCl_2$ aqueous solutions, simulated K_S values range from 0.07 to 0.20 kg.mol^{-1}. Considering uncertainties on simulated K_H values, simulated K_S are in agreement with estimations obtained using the Schumpe and Weisenberger model with predicted K_S in between -0.02 and 0.28 kg.mol^{-1} for the same systems [88, 89].

3.7. Solubility of sulphur dioxide in brines

We propose to supplement information contained in Tables 15 and 16 computing SO_2 solubility in NaCl and $CaCl_2$ aqueous solutions at higher pressure values. For the two investigated temperatures (298.15 K and 323.15 K), phase diagrams for the SO_2 + brine mixtures exhibit a VL equilibrium domain at the lowest pressures and a liquid-liquid equilibrium domain at the highest pressures, with a three-phase line in between these two domains. MC molecular simulations were performed in the Gibbs ensemble for pressures up to 10 MPa, in the Gibbs-NpT ensemble for diphasic systems and in the Gibbs-NVT ensemble for triphasic systems. Note that an additional constraint prevents the transfer of ions from the liquid to the vapour phase. For each MC simulation, the number of generated configurations ranged within 7.10^8 and 8.10^8 including the equi-

Table 16: Simulated Henry constants for some gases in $CaCl_2$ aqueous solutions for temperatures ranging from 323.15 K to 373.15 K.

Temperature	m	Henry constant (MPa.mol/mol)				
(K)	(mol.kg^{-1})	SO_2	CO_2	NO	O_2	N_2
298.15	1	43	643	8155	9208	27339
	2	67	942	10880	12387	36286
	3	72	1587	18655	21145	63282
323.15	1	47	825	8723	9861	25073
	2	53	1237	12593	14174	37067
	3	60	1862	15225	17495	45923
373.15	1	123	1533	9722	10816	24196
	2	189	2441	14181	15793	36816
	3	253	3115	18332	20281	46899

libration of the system and the production run. Table 17 presents simulated phase compositions for SO_2 + brines (H_2O/NaCl and $H_2O/CaCl_2$, 3 mol.kg^{-1}) systems for temperatures in between 298.15 K and 373.15 K. Table 17 contains information regarding coordinates of the three-phase line in between the vapour-liquid and the liquid-liquid equilibrium domains in the case of NaCl brines. For these systems, obtained three-phase line pressures are similar to pure water cases with 0.40 MPa and 0.89 MPa at 298.15 K and 323.15 K, respectively. Note that no attempt to capture the three-phase line has been done in the case of SO_2 + $H_2O/CaCl_2$ systems. Using solubility data presented in Table 17, one can estimate Henry constant values of SO_2 in a NaCl (3 mol.kg^{-1}) aqueous solution: 41 MPa.mol/mol at 298.15 K and 72 MPa.mol/mol at 323.15 K, in agreement with values reported in Table 15. Using solubility data presented in Table 17, one can also estimate Henry constant values for SO_2 in a $CaCl_2$ (3 mol.kg^{-1}) aqueous solutions: 51 MPa.mol/mol at 298.15 K, 59 MPa.mol/mol at 323.15 K and 257 MPa.mol/mol at 373.15 K, in agreement with values reported in Table 16.

Table 17: Phase compositions for the SO_2 + brine (H_2O/NaCl and H_2O/$CaCl_2$, with a salt molal concentration of 3 mol.kg^{-1}) systems at different temperatures, obtained using MC molecular simulation. V denotes the vapour phase, and L1 and L2 stand for H_2O-rich and SO_2-rich liquids, respectively.

P	Molar fraction of SO_2			P	Molar fraction of SO_2		
(MPa)	L1	L2	V	(MPa)	L1	L2	V
	H_2O + NaCl, 298.15 K				H_2O + $CaCl_2$, 298.15 K		
0.05	0.0012	—	0.9862	0.05	0.0022	—	0.9877
0.10	0.0035	—	0.9935	0.10	0.0036	—	0.9945
0.50	0.0124	—	0.9986	0.50	0.0112	—	0.9986
0.40	0.0107	0.9912	0.9984	1.00	0.0321	0.9916	—
1.00	0.0198	0.9926	—		H_2O + $CaCl_2$, 323.15 K		
3.00	0.0202	0.9923	—	0.05	0.0004	—	0.9434
5.00	0.0382	0.9878	—	0.10	0.0014	—	0.9725
10.00	0.0120	0.9929	—	0.50	0.0081	—	0.9937
	H_2O + NaCl, 323.15 K			1.00	0.0268	0.9858	—
0.05	0.0008	—	0.9407		H_2O + $CaCl_2$, 373.15 K		
0.10	0.0013	—	0.9699	0.05	0.0001	—	0.3737
0.50	0.0074	—	0.9932	0.10	0.0003	—	0.6724
0.89	0.0123	0.9844	0.9960	0.50	0.0018	—	0.9321
1.00	0.0135	0.9846	—	1.00	0.0157	0.9604	—
3.00	0.0132	0.9856	—				
5.00	0.0133	0.9849	—				
10.00	0.0101	0.9843	—				

4. Conclusions

In the present work, we have proposed new insights for NO + SO_2 binary systems, using molecular simulation techniques, equations of state, and experiments. Using intermolecular potentials available in the literature we have demonstrated the capability of molecular simulation techniques in predicting properties for mixtures. Solubilities of some gases (CO_2 and associated gases such as O_2, N_2, SO_2, NO) in water and in NaCl and $CaCl_2$ aqueous solutions have also been studied using molecular simulation techniques. In the case of the highest soluble gases (*e.g.*, sulphur dioxide) reasonable simulation box size can be envisaged and explicit analysis of phase compositions performed. For gas with low solubility value (CO_2, O_2, N_2, and NO) we only determined Henry constants.

Results of performed quantum chemical calculations tend to indicate no favoured chemical reaction between NO and SO_2 in the gas phase. In addition, no evidence of such chemical reaction has been observed during the experimental data acquisition. New sets of experimental vapour compositions have been proposed for NO + SO_2 binary mixtures. Data generated using molecular simulations agree fairly well with reference experimental data. Using the so-obtained data, we proposed new sets of parameters for the PPR78 EoS model. Henry constant values for gases in water generated by means of molecular simulations fairly agree with reference data. The performed study on the ability of various potentials in predicting sodium chloride and calcium chloride brine densities and osmotic pressures led us to recommend two sets of parameters, both involving the TIP4P/2005 water potential. Finally, Henry constant values for gases in sodium chloride and calcium chloride brines were generated by means of molecular simulations.

In this work, we show that combining some experiments, molecular simulations and equation of state modelling is relevant to fill the lack of information for gas mixtures representative of systems encountered in CCS operations. Using validated intermolecular potentials, molecular simulations is an interesting

tool to generate data, especially when hazardous compounds and/or extreme pressure or temperature conditions are considered. Simulated data can then be used to optimize equations of state parameters, and thus to improve models implemented within geochemical codes.

Acknowledgement

The financial support from the French Agence Nationale de la Recherche, ANR, for the SIGARRR project (ANR-13-SEED-006) is gratefully acknowledged. Authors would like to thank Dr Bernard Rousseau for the use of the NEWTON Molecular Dynamics code.

References

[1] United Nation Framework Convention on Climate Change, Adoption of the Paris Agreement, Technical Report, 2015.

[2] A. Torvanger, M. T. Lund, N. Rive, Carbon capture and storage deployment rates: needs and feasibility, Mitigation and Adaptation Strategies for Global Change 18 (2013) 187–205.

[3] S. Thibeau, P. Chiquet, G. Mouronval, M. Lescanne, Geochemical assessment of the injection of CO_2 into rousse depleted gas reservoir, Energy Procedia 1 (2009) 3383–3390.

[4] M. Lescanne, J. Hy-Billiot, N. Aimard, C. Prinet, The site monitoring of the Lacq industrial CCS reference project, Energy Procedia 4 (2011) 3518–3525.

[5] B. Garcia, J. Hy-Billiot, V. Rouchon, G. Mouronval, M. Lescanne, V. Lachet, N. Aimard, A geochemical approach for monitoring a CO_2 pilot site: Rousse, france. a major gases, CO_2 - carbon isotopes and noble gases combined approach, Oil & Gas Science and Technology – Revue d'IFP Energies nouvelles 67 (2012) 341–353.

[6] B. Creton, T. d. Bruin, D. Le Roux, P. Duchet-Suchaux, V. Lachet, Impact of associated gases on equilibrium and transport properties of a CO_2 stream: Molecular simulation and experimental studies, International Journal of Thermophysics 35 (2014) 256–276.

[7] J. Sterpenich, J. Dubessy, J. Pironon, S. Renard, M.-C. Caumon, A. Randi, J.-N. Jaubert, E. Favre, D. Roizard, M. Parmentier, M. Azaroual, V. Lachet, B. Creton, T. Parra, E. E. Ahmar, C. Coquelet, V. Lagneau, J. Corvisier, P. Chiquet, Role of impurities on CO_2 injection: Experimental and numerical simulations of thermodynamic properties of water-salt-gas mixtures (CO_2 + co-injected gases) under geological storage conditions, Energy Procedia 37 (2013) 3638–3645.

[8] J. Corvisier, E. E. Ahmar, C. Coquelet, J. Sterpenich, R. Privat, J.-N. Jaubert, K. Ballerat-Busserolles, J.-Y. Coxam, P. Cézac, F. Contamine, J.-P. Serin, V. Lachet, B. Creton, M. Parmentier, P. Blanc, L. André, L. d. Lary, E. C. Gaucher, Simulations of the impact of co-injected gases on CO_2 storage, the SIGARRR project: First results on water-gas interactions modeling, Energy Procedia 63 (2014) 3160–3171.

[9] J. Corvisier, M. Hajiw, E. El Ahmar, C. Coquelet, J. Sterpenich, R. Privat, J.-N. Jaubert, K. Ballerat-Busserolles, J.-Y. Coxam, P. Cézac, F. Contamine, J.-P. Serin, V. Lachet, B. Creton, M. Parmentier, J. Tremosa, P. Blanc, L. André, L. de Lary, E. Gaucher, Simulations of the impact of co-injected gases on CO_2 storage, the SIGARRR project: Processes and geochemical approaches for gas-water-salt interactions modeling, Energy Procedia 114 (2017) 3322–3334. 13th International Conference on Greenhouse Gas Control Technologies, GHGT-13, 14-18 November 2016, Lausanne, Switzerland.

[10] A. Estublier, P. Bachaud, A. Michel, N. Maurand, J.-P. Deflandre, Long-term fate of CO_2 in a saline aquifer: modeling issues, Energy Procedia 63 (2014) 3464–3474.

[11] C. Haase, A. Dahmke, M. Ebert, D. Schäfer, F. Dethlefsen, Suitability of existing numerical model codes and thermodynamic databases for the prognosis of calcite dissolution processes in near-surface sediments due to a CO_2 leakage investigated by column experiments, Aquatic Geochemistry 20 (2014) 639–661.

[12] C. Haase, M. Ebert, F. Dethlefsen, Uncertainties of geochemical codes and thermodynamic databases for predicting the impact of carbon dioxide on geologic formations, Applied Geochemistry 67 (2016) 81–92.

[13] D.-Y. Peng, D. B. Robinson, A new two-constant equation of state, Industrial & Engineering Chemistry Fundamentals 15 (1976) 59–64.

[14] H. Li, J. P. Jakobsen, Ø. Wilhelmsen, J. Yan, Pvtxy properties of CO_2 mixtures relevant for CO_2 capture, transport and storage: Review of available experimental data and theoretical models, Applied Energy 88 (2011) 3567–3579.

[15] H. Li, Ø. Wilhelmsen, Y. Lv, W. Wang, J. Yan, Viscosities, thermal conductivities and diffusion coefficients of CO_2 mixtures: Review of experimental data and theoretical models, International Journal of Greenhouse Gas Control 5 (2011) 1119–1139.

[16] X. Xu, R. Privat, J.-N. Jaubert, Addition of the sulfur dioxide group (SO_2), the oxygen group (O_2), and the nitric oxide group (NO) to the E-PPR78 model, Industrial & Engineering Chemistry Research 54 (2015) 9494–9504.

[17] X. Xu, R. Privat, J.-N. Jaubert, V. Lachet, B. Creton, Phase equilibrium of CCS mixtures: Equation of state modeling and monte carlo simulation, The Journal of Supercritical Fluids 119 (2017) 169–202.

[18] E. Bourasseau, V. Lachet, N. Desbiens, J.-B. Maillet, J.-M. Teuler, P. Ungerer, Thermodynamic behavior of the CO_2 + NO_2/N_2O_4 mixture: a monte carlo simulation study, The Journal of Physical Chemistry B 112 (2008) 15783–15792.

[19] V. Lachet, T. de Bruin, P. Ungerer, C. Coquelet, A. Valtz, V. Hasanov, F. Lockwood, D. Richon, Thermodynamic behavior of the CO_2+SO_2 mixture: Experimental and monte carlo simulation studies, Energy Procedia 1 (2009) 1641–1647.

[20] E. El Ahmar, B. Creton, A. Valtz, C. Coquelet, V. Lachet, D. Richon, P. Ungerer, Thermodynamic study of binary systems containing sulphur dioxide: Measurements and molecular modelling, Fluid Phase Equilibria 304 (2011) 21–34.

[21] V. Lachet, B. Creton, T. de Bruin, E. Bourasseau, N. Desbiens, Ø. Wilhelmsen, M. Hammer, Equilibrium and transport properties of CO_2+N_2O

and CO_2+NO mixtures: Molecular simulation and equation of state modelling study, Fluid Phase Equilibria 322-323 (2012) 66–78.

[22] C. Coquelet, A. Valtz, P. Arpentinier, Thermodynamic study of binary and ternary systems containing CO_2 + impurities in the context of CO_2 transportation, Fluid Phase Equilibria 382 (2014) 205–211.

[23] ARMINES, Patent no fr 2 853 414, procédé et dispositif pour prélever des micro échantillons d'un fluide sous pression contenu dans un container, 2003.

[24] S. Lasala, P. Chiesa, R. Privat, J.-N. Jaubert, VLE properties of CO_2-based binary systems containing N_2, O_2 and Ar: Experimental measurements and modelling results with advanced cubic equations of state, Fluid Phase Equilibria 428 (2016) 18–31.

[25] S. Lasala, P. Chiesa, R. Privat, J.-N. Jaubert, Measurement and prediction of multi-property data of CO_2-N_2-O_2-CH_4 mixtures with the Peng-Robinson +residual Helmholtz energy-based model, Fluid Phase Equilibria 437 (2017) 166–180.

[26] S. Lasala, P. Chiesa, R. Privat, J.-N. Jaubert, Modeling the thermodynamics of fluids treated by CO_2 capture processes with Peng-Robinson +residual Helmholtz energy-based mixing rules, Industrial & Engineering Chemistry Research 56 (2017) 2259–2276.

[27] Y. Le Guennec, S. Lasala, R. Privat, J.-N. Jaubert, A consistency test for α-functions of cubic equations of state, Fluid Phase Equilibria 427 (2016) 513–538.

[28] Y. Le Guennec, R. Privat, J.-N. Jaubert, Development of the translated-consistent tc-pr and tc-rk cubic equations of state for a safe and accurate prediction of volumetric, energetic and saturation properties of pure compounds in the sub- and super-critical domains, Fluid Phase Equilibria 429 (2016) 301–312.

[29] Y. Le Guennec, R. Privat, S. Lasala, J.-N. Jaubert, On the imperative need to use a consistent α-function for the prediction of pure-compound supercritical properties with a cubic equation of state, Fluid Phase Equilibria 445 (2017) 45– 53.

[30] J.-N. Jaubert, R. Privat, Y. Le Guennec, L. Coniglio, Note on the properties altered by application of a péneloux-type volume translation to an equation of state, Fluid Phase Equilibria 419 (2016) 88–95.

[31] R. Privat, J.-N. Jaubert, Y. Le Guennec, Incorporation of a volume translation in an equation of state for fluid mixtures: which combining rule? which effect on properties of mixing?, Fluid Phase Equilibria 427 (2016) 414–420.

[32] X. Xu, S. Lasala, R. Privat, J.-N. Jaubert, E-PPR78: A proper cubic EoS for modelling fluids involved in the design and operation of carbon dioxide capture and storage (CCS) processes, International Journal of Greenhouse Gas Control 56 (2017) 126–154.

[33] J.-N. Jaubert, F. Mutelet, VLE predictions with the Peng-Robinson equation of state and temperature dependent kij calculated through a group contribution method, Fluid Phase Equilibria 224 (2004) 285–304.

[34] J.-W. Qian, R. Privat, J.-N. Jaubert, Predicting the phase equilibria, critical phenomena, and mixing enthalpies of binary aqueous systems containing alkanes, cycloalkanes, aromatics, alkenes, and gases (N_2, CO_2, H_2S, H_2) with the PPR78 equation of state, Industrial & Engineering Chemistry Research 52 (2013) 16457–16490.

[35] P. Ungerer, B. Tavitian, A. Boutin, Applications of Molecular Simulation in the Oil and Gas Industry - Monte-Carlo Methods, Editions TECHNIP, 2005.

[36] A. Z. Panagiotopoulos, Direct determination of phase coexistence prop-

erties of fluids by Monte Carlo simulation in a new ensemble, Molecular Physics 61 (1987) 813–826.

[37] A. Panagiotopoulos, N. Quirke, M. Stapleton, D. J. Tildesley, Phase equilibria by simulation in the Gibbs ensemble, Molecular Physics 63 (1988) 527–545.

[38] S. Duane, A. Kennedy, B. J. Pendleton, D. Roweth, Hybrid Monte Carlo, Physics Letters B 195 (1987) 216–222.

[39] V. Lachet, J.-M. Teuler, B. Rousseau, Classical force field for hydrofluorocarbon molecular simulations. application to the study of gas solubility in poly(vinylidene fluoride), The Journal of Physical Chemistry A 119 (2015) 140–151.

[40] N.-T. Van-Oanh, C. Houriez, B. Rousseau, Viscosity of the 1-ethyl-3-methylimidazolium bis(trifluoromethylsulfonyl)imide ionic liquid from equilibrium and nonequilibrium molecular dynamics, Physical Chemistry Chemical Physics 12 (2010) 930–936.

[41] Y. Luo, B. Roux, Simulation of osmotic pressure in concentrated aqueous salt solutions, The Journal of Physical Chemistry Letters 1 (2010) 183–189.

[42] J. G. Harris, K. H. Yung, Carbon dioxide's liquid-vapor coexistence curve and critical properties as predicted by a simple molecular model, The Journal of Physical Chemistry 99 (1995) 12021–12024.

[43] J. Delhommelle, Etablissement de potentiels d'interactions pour la simulation moléculaire. Application à la prédiction des équilibres liquide-vapeur de mélanges binaires alcane-molécule multipolaire, Ph.D. Thesis, Université Paris XI, Orsay, France, 2000.

[44] J. Vrabec, J. Stoll, H. Hasse, A set of molecular models for symmetric quadrupolar fluids, The Journal of Physical Chemistry B 105 (2001) 12126–12133.

[45] Y. Boutard, P. Ungerer, J. M. Teuler, M. G. Ahunbay, S. F. Sabater, J. Pérez-Pellitero, A. D. Mackie, E. Bourasseau, Extension of the anisotropic united atoms intermolecular potential to amines, amides and alkanols, Fluid Phase Equilibria 236 (2005) 25–41.

[46] H. J. C. Berendsen, J. R. Grigera, T. P. Straatsma, The missing term in effective pair potentials, The Journal of Physical Chemistry 91 (1987) 6269–6271.

[47] J. L. F. Abascal, C. Vega, A general purpose model for the condensed phases of water: TIP4P/2005, The Journal of Chemical Physics 123 (2005) 234505.

[48] C. Nieto-Draghi, T. de Bruin, J. Pérez-Pellitero, J. Bonet Avalos, A. D. Mackie, Thermodynamic and transport properties of carbon dioxide from molecular simulation, The Journal of Chemical Physics 126 (2007) 064509.

[49] B. Guillot, A reappraisal of what we have learnt during three decades of computer simulations on water, Journal of Molecular Liquids 101 (2002) 219–260.

[50] L. Vlcek, A. A. Chialvo, D. R. Cole, Optimized unlike-pair interactions for water-carbon dioxide mixtures described by the SPC/E and EPM2 models, The Journal of Physical Chemistry B 115 (2011) 8775–8784.

[51] C. Vega, J. L. F. Abascal, Simulating water with rigid non-polarizable models: a general perspective, Physical Chemistry Chemical Physics 13 (2011) 19663?19688.

[52] R. Sakamaki, A. K. Sum, T. Narumi, K. Yasuoka, Molecular dynamics simulations of vapor/liquid coexistence using the nonpolarizable water models, The Journal of Chemical Physics 134 (2011) 124708.

[53] V. Vinš, D. Celný, B. Planková, T. Němec, M. Duška, J. Hrubý, P. Dančová, M. Veselý, Molecular simulations of the vapor-liquid phase

889 interfaces of pure water modeled with the SPC/E and the TIP4P/2005
890 molecular models, EPJ Web of Conferences 114 (2016) 02136.

891 [54] J. Chandrasekhar, D. C. Spellmeyer, W. L. Jorgensen, Energy compo-
892 nent analysis for dilute aqueous solutions of lithium(1+), sodium(1+),
893 fluoride(1-), and chloride(1-) ions, Journal of the American Chemical So-
894 ciety 106 (1984) 903–910.

895 [55] W. L. Jorgensen, D. S. Maxwell, J. Tirado-Rives, Development and testing
896 of the OPLS all-atom force field on conformational energetics and properties
897 of organic liquids, Journal of the American Chemical Society 118 (1996)
898 11225–11236.

899 [56] D. R. Wheeler, J. Newman, Molecular dynamics simulations of multicom-
900 ponent diffusion. 1. equilibrium method, The Journal of Physical Chemistry
901 B 108 (2004) 18353–18361.

902 [57] G. H. Goo, G. Sung, S. H. Lee, Molecular dynamics simulation studies of
903 the limiting conductances of $MgCl_2$ and $CaCl_2$ in supercritical water using
904 SPC/E model for water, Molecular Simulation 30 (2004) 37–44.

905 [58] J. Åqvist, Ion-water interaction potentials derived from free energy per-
906 turbation simulations, The Journal of Physical Chemistry 94 (1990) 8021–
907 8024.

908 [59] M. M. Reif, P. H. Hünenberger, Computation of methodology-independent
909 single-ion solvation properties from molecular simulations. IV. optimized
910 lennard-jones interaction parameter sets for the alkali and halide ions in
911 water, The Journal of Chemical Physics 134 (2011) 144104.

912 [60] J.-C. Neyt, A. Wender, V. Lachet, A. Ghoufi, P. Malfreyt, Prediction
913 of the concentration dependence of the surface tension and density of salt
914 solutions: atomistic simulations using drude oscillator polarizable and non-
915 polarizable models, Physical Chemistry Chemical Physics 15 (2013) 11679–
916 11690.

[61] J.-C. Neyt, A. Wender, V. Lachet, A. Szymczyk, A. Ghoufi, P. Malfreyt, How does the electronic continuum model perform in the prediction of the surface tension of salt solutions?, Chemical Physics Letters 595-596 (2014) 209–213.

[62] G. A. Orozco, O. A. Moultos, H. Jiang, I. G. Economou, A. Z. Panagiotopoulos, Molecular simulation of thermodynamic and transport properties for the H_2O+NaCl system, The Journal of Chemical Physics 141 (2014) 234507.

[63] E. S. Tsai, H. Jiang, A. Z. Panagiotopoulos, Monte carlo simulations of H_2O–$CaCl_2$ and H2O–$CaCl_2$–CO_2 mixtures, Fluid Phase Equilibria 407 (2016) 262–268.

[64] R. P. Matthews, K. J. Naidoo, Experimentally consistent ion association predicted for metal solutions from free energy simulations, The Journal of Physical Chemistry B 114 (2010) 7286–7293.

[65] L. X. Dang, D. E. Smith, Comment on "mean force potential for the calcium–chloride ion pair in water" [j. chem. phys. 99, 4229 (1993)], The Journal of Chemical Physics 102 (1995) 3483.

[66] L. X. Dang, Mechanism and thermodynamics of ion selectivity in aqueous solutions of 18-crown-6 ether: A molecular dynamics study, Journal of the American Chemical Society 117 (1995) 6954–6960.

[67] M. Předota, Z. Zhang, P. Fenter, D. J. Wesolowski, P. T. Cummings, Electric double layer at the rutile (110) surface. 2. adsorption of ions from molecular dynamics and X-ray experiments, The Journal of Physical Chemistry B 108 (2004) 12061–12072.

[68] M. J. Frisch, G. W. Trucks, H. B. Schlegel, G. E. Scuseria, M. A. Robb, Cheeseman, G. Scalmani, V. Barone, B. Mennucci, G. A. Petersson, H. Nakatsuji, M. Caricato, X. Li, H. P. Hratchian, Izmaylov, A. F.,

J. Bloino, G. Zheng, Sonnenberg, J. L., M. Hada, M. Ehara, K. Toyota, R. Fukuda, J. Hasegawa, M. Ishida, T. Nakajima, Y. Honda, O. Kitao, H. Nakai, T. Vreven, J. A. Montgomery, Peralta, J. E., F. Ogliaro, M. Bearpark, Heyd, J. J., E. Brothers, K. N. Kudin, Staroverov, V. N., R. Kobayashi, J. Normand, K. Raghavachari, A. Rendell, J. C. Burant, S. S. Iyengar, J. Tomasi, M. Cossi, N. Rega, J. M. Millam, M. Klene, J. E. Knox, J. B. Cross, V. Bakken, C. Adamo, J. Jaramillo, R. Gomperts, R. E. Stratmann, O. Yazyev, A. J. Austin, R. Cammi, C. Pomelli, J. W. Ochterski, R. L. Martin, K. Morokuma, V. G. Zakrzewski, G. A. Voth, P. Salvador, J. J. Dannenberg, S. Dapprich, A. D. Daniels, Farkas, J. B. Foresman, J. V. Ortiz, J. Cioslowski, D. J. Fox, Gaussian 09, revision b.01, Gaussian 09, Revision B.01, Gaussian, Inc., Wallingford CT (2009).

[69] Y. Zhao, D. G. Truhlar, The M06 suite of density functionals for main group thermochemistry, thermochemical kinetics, noncovalent interactions, excited states, and transition elements: two new functionals and systematic testing of four M06-class functionals and 12 other function, Theoretical Chemistry Accounts 120 (2007) 215–241.

[70] M. Tobita, S. Perera, M. Musial, R. Bartlett, M. Nooijen, J. Lee, Critical comparison of single-reference and multireference coupled-cluster methods: Geometry, harmonic frequencies, and excitation energies of N_2O_2, The Journal of Chemical Physics 119 (2003) 10713–10723.

[71] R. Sayós, R. Valero, J. Anglada, M. González, Theoretical investigation of the eight low-lying electronic states of the cis- and trans-nitric oxide dimers and its isomerization using multiconfigurational second-order perturbation theory (CASPT2), The Journal of Chemical Physics 112 (2000) 6608–6624.

[72] A. Dkhissi, P. Soulard, A. Perrin, N. Lacome, The 5NO6 dimer, Journal of Molecular Spectroscopy 183 (1997) 12–17.

[73] A. McKellar, J. Watson, B. Howard, The NO dimer: 15 N isotopic infrared spectra, line-widths, and force field, Molecular Physics 86 (1995) 273–286.

[74] M. P. Allen, D. J. Tildesley, Computer simulation of liquids, Oxford Science Publications, Oxford, 1987.

[75] R. Privat, J.-N. Jaubert, Classification of global fluid-phase equilibrium behaviors in binary systems, Chemical Engineering Research and Design 91 (2013) 1807–1839.

[76] P. Van Konynenburg, R. Scott, Critical lines and phase equilibria in binary van der waals mixtures, Philosophical Transactions of the Royal Society: Mathematical, Physical and Engineering Sciences 298 (1980) 495–540.

[77] M. Michelsen, A modified Huron-Vidal mixing rule for cubic equations of state, Fluid Phase Equilibria 60 (1990) 213–219.

[78] M. Lísal, W. R. Smith, K. Aim, Analysis of Henry's constant for carbon dioxide in water via Monte Carlo simulation, Fluid Phase Equilibria 226 (2004) 161–172.

[79] G. A. Orozco, V. Lachet, A. D. Mackie, Physical absorption of green house gases in amines: The influence of functionality, structure, and cross-interactions, The Journal of Physical Chemistry B 120 (2016) 13136–13143.

[80] J. J. Carroll, J. D. Slupsky, A. E. Mather, The solubility of carbon dioxide in water at low pressure, Journal of Physical and Chemical Reference Data 20 (1991) 1201–1209.

[81] A. Harvey, Semiempirical correlation for henry's constants over large temperature ranges, AIChE Journal 42 (1996) 1491–1494.

[82] C. L. Yaws, Chemical properties handbook: physical, thermodynamic, environmental transport, safety, and health related properties for organic and inorganic chemicals, McGraw-Hill, New York, USA, 1999.

[83] H.-L. Zhang, S.-J. Han, Viscosity and density of water + sodium chloride + potassium chloride solutions at 298.15 K, Journal of Chemical & Engineering Data 41 (1996) 516–520.

[84] G. Wilczek-Vera, J. H. Vera, How much do we know about the activity of individual ions?, The Journal of Chemical Thermodynamics 99 (2016) 65–69.

[85] B. Staples, R. Nuttall, The activity and osmotic coefficients of aqueous calcium chloride at 298.15 K, Journal of Physical and Chemical Reference Data 6 (1977) 385–408.

[86] I. M. Sechenov, Über die konstitution der salzlösungen auf grund ihres verhaltens zu kohlensäurethe solubility of carbon dioxide in water at low pressure, Zeitschrift fr Physikalische Chemie 4 (1889) 117–125.

[87] S. K. Saxena, Advances in Physical Geochemistry, vol. 2, Springer New York, 1982.

[88] A. Schumpe, The estimation of gas solubilities in salt solutions, Chemical Engineering Science 48 (1993) 153–158.

[89] S. Weisenberger, A. Schumpe, Estimation of gas solubilities in salt solutions at temperatures from 273 K to 363 K, AIChE Journal 42 (1996) 298–300.

[90] W. B. Campbell, O. Maass, Equilibria in sulfur dioxide solutions, Canadian Journal of Research, Section B 2 (1930) 42–64.

[91] T. K. Sherwood, Solubilities of sulfur dioxide and ammonia in water, Industrial & Engineering Chemistry 17 (1925) 745–747.

[92] B. Rumpf, G. Maurer, Solubilities of hydrogen cyanide and sulfur dioxide in water at temperatures from 293.15 to 413.15 K and pressures up to 2.5 MPa, Fluid Phase Equilibria 81 (1992) 241–260.

[93] S. G. Sayegh, J. Najman, CO_2 - SO_2 brine phase behavior studies, Report (1984).

[94] H.-L. Zhang, G.-H. Chen, S.-J. Han, Viscosity and density of H_2O+NaCl+$CaCl_2$ and H_2O+KCl+$CaCl_2$ at 298.15 K, Journal of Chemical & Engineering Data 42 (1997) 526–530.

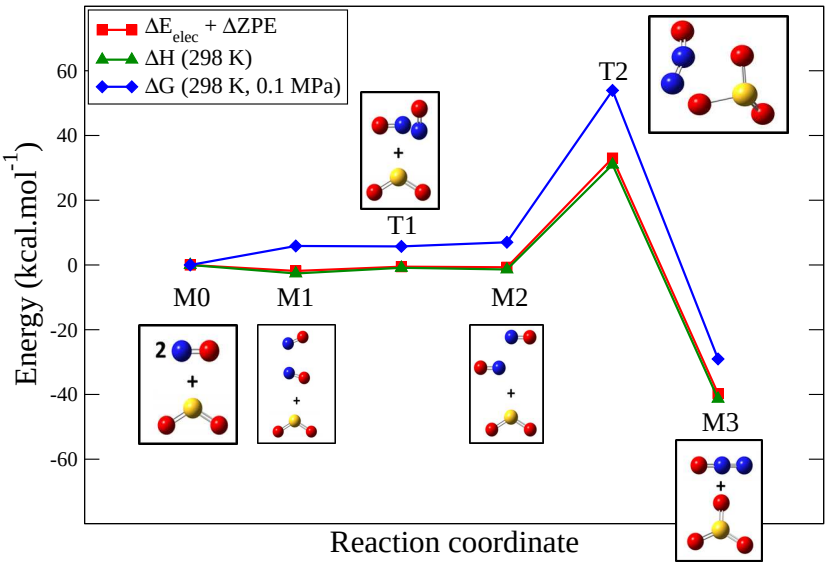

Figure 1: Energy profiles for the $SO_2 + 2NO \rightleftharpoons SO_3 + N_2O$ reaction for the electronic energy corrected for the zero point energy (red), the enthalpy at T = 298 K (green) and the Gibbs energy at T = 298 K and P = 0.1 MPa (blue).

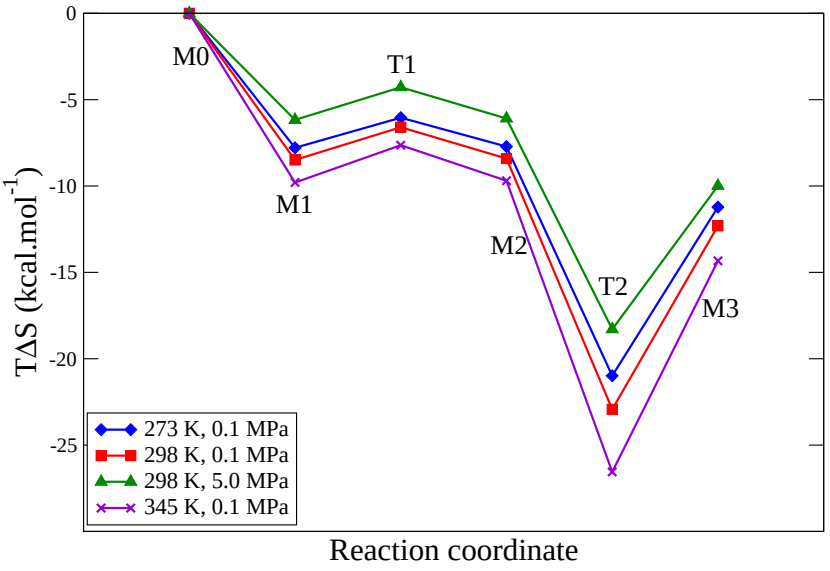

Figure 2: Changes (in kcal.mol^{-1}) of TΔS as a function of the reaction coordinate with respect to M0, for 3 temperatures and 2 pressures.

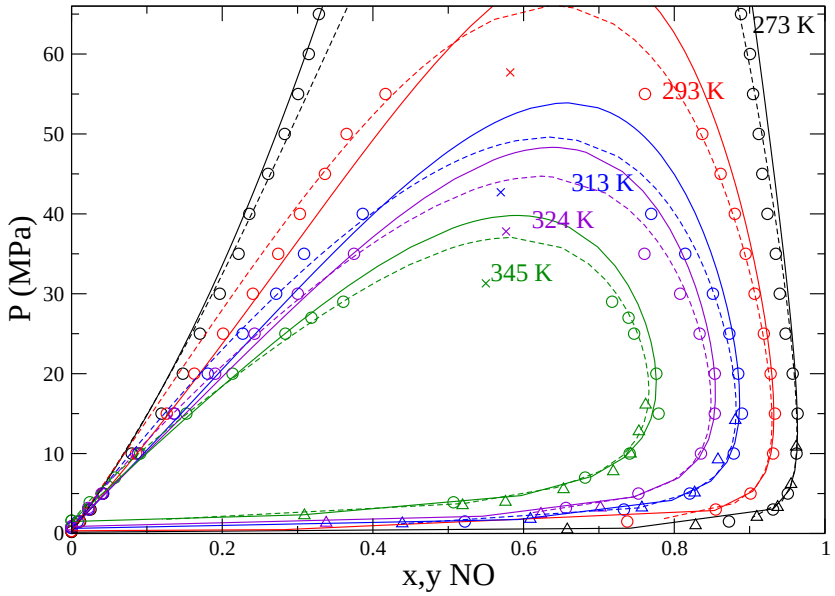

Figure 3: (P, x, y) phase diagrams for the NO + SO_2 at five temperatures: 273 K (black), 293 K (red), 313 K (blue), 324 K (purple), and 345 K (green). Triangles stand for experimental data (this work and data cited in [16]). Circles denote data obtained using MC molecular simulations, and crosses represent critical points estimated using equations (9) and (10). Lines represent predictions obtained using the PR EoS together with the van Laar model (solid line) and the PR EoS together with the residual part of the Wilson model (dashed line).

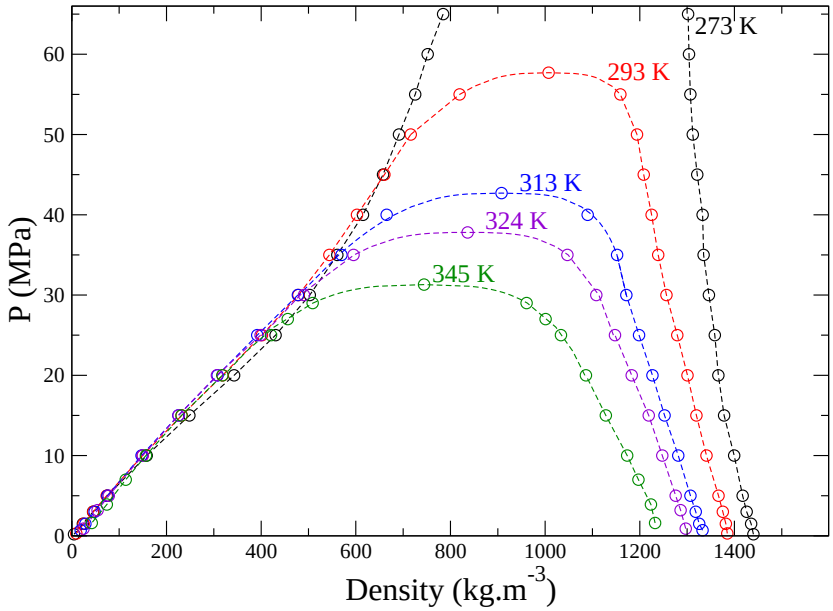

Figure 4: Pressure-density diagrams drawn using data obtained by MC molecular simulations, for the NO + SO_2 at five temperatures: 273 K, 293 K, 313 K, 324 K, and 345 K.

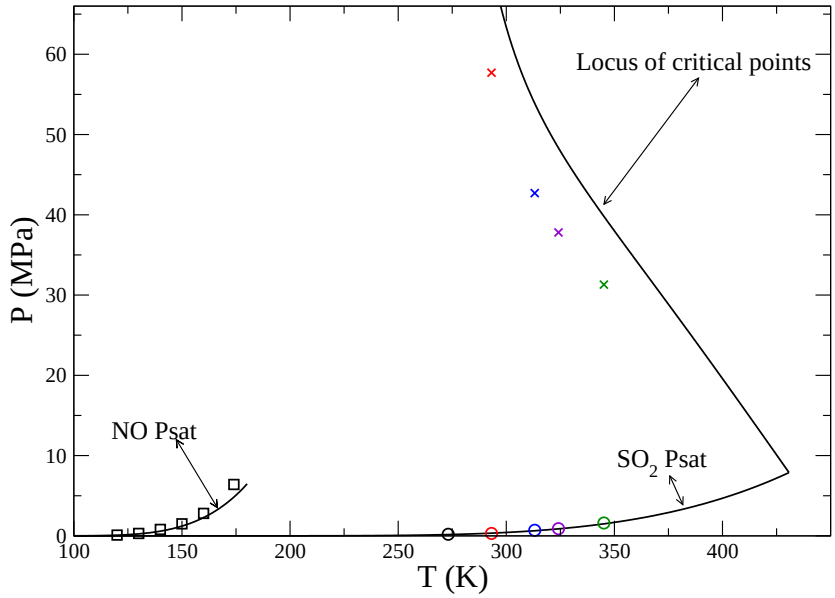

Figure 5: Global pressure-temperature diagram for the NO + SO_2. Lines represent predictions using the PR EoS with the the van Laar model, and symbols stands for data obtained using MC molecular simulations at five temperatures: 273 K (black), 293 K (red), 313 K (blue), 324 K (purple), and 345 K (green). NO data for vapour pressure (squares) obtained by MC simulations are taken from our previous work [21].

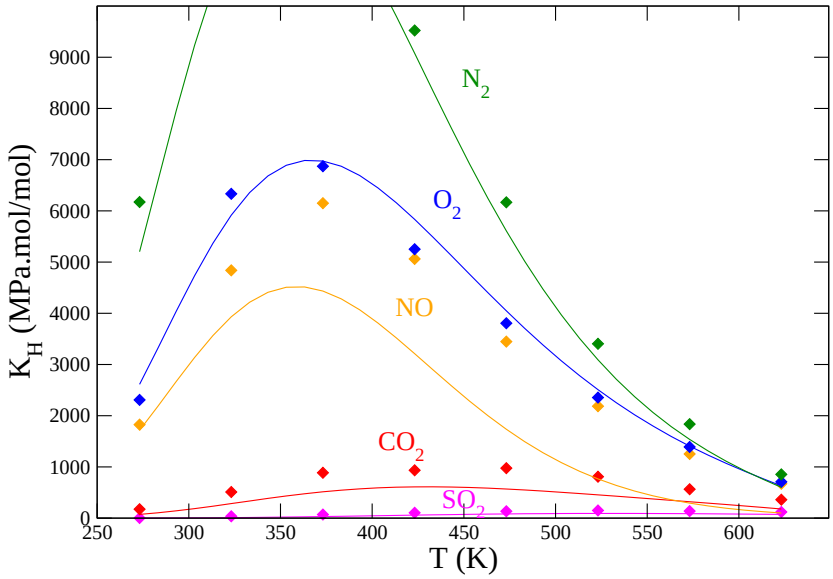

Figure 6: Comparison of simulated Henry constants (diamonds) for SO_2, CO_2, NO, O_2, and N_2 in water, and corresponding curve fitting of experimental values (lines).

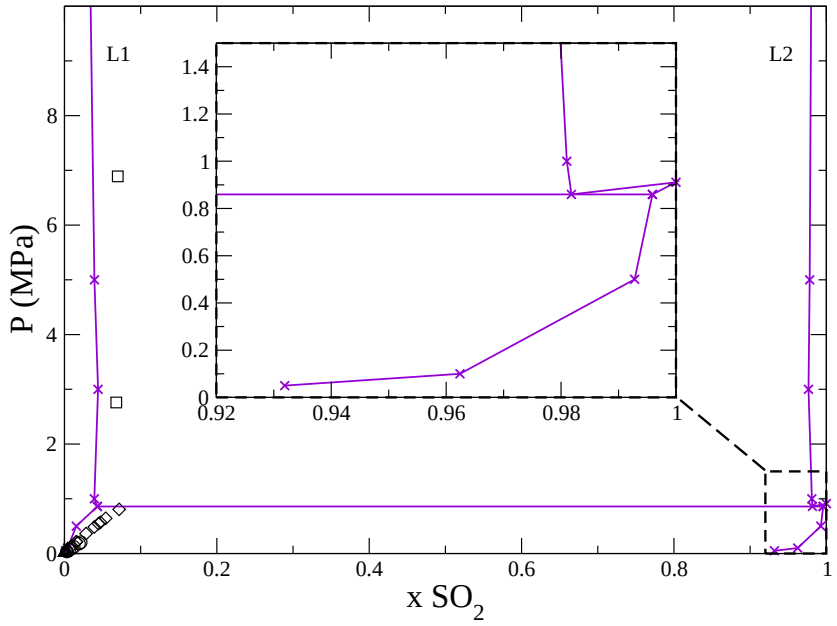

Figure 7: Phase diagrams for SO_2 + H_2O binary mixtures obtained using MC molecular simulations at 323 K (crosses) for pressures up to 10 MPa, and a zoom is proposed on the SO_2-rich region for pressures up to 1.5 MPa. Experimental data for the H_2O-rich region were extracted from works of Campbell (circles) [90], Sherwood (triangles up) [91], Rumpf (diamonds) [92] and Sayegh (squares) [93], measured at 323 K, 323 K, 333 K, and 318 K, respectively.

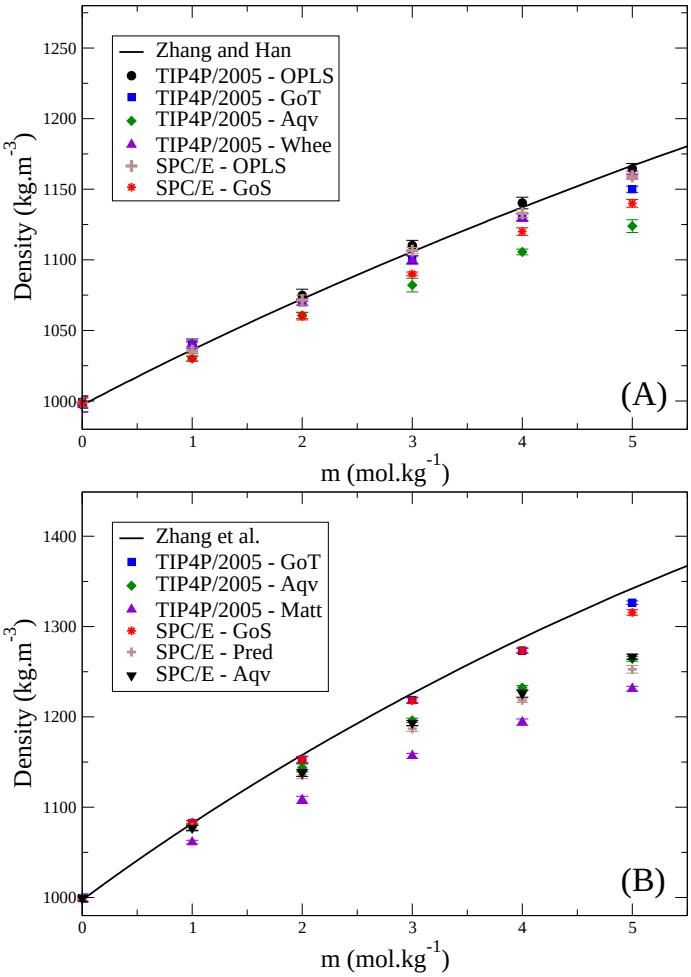

Figure 8: Predicted density values for (A) NaCl (see Table 12) and (B) $CaCl_2$ (see Table 13) aqueous solutions as a function of the salt molal concentration, at 298 K and 0.1 MPa. The line represents experimental values extracted (A) from the work by Zhang and Han [83] and (B) from the work by Zhang *et al.* [94].

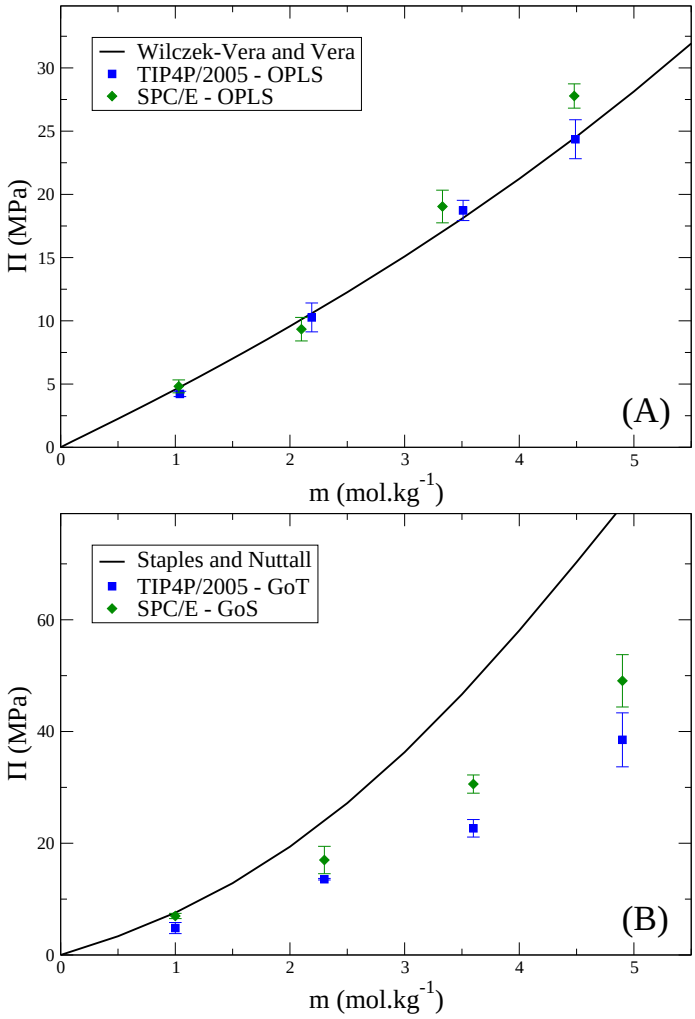

Figure 9: Comparison of experimental and predicted osmotic pressure values for (A) NaCl and (B) $CaCl_2$ aqueous solutions as a function of the salt molal concentration, at 298 K (see values in Table 14). The line represents experimental values extracted (A) from the work by Wilczek-Vera and Vera [84] and (B) data converted from the work by Staples and Nuttall [85].

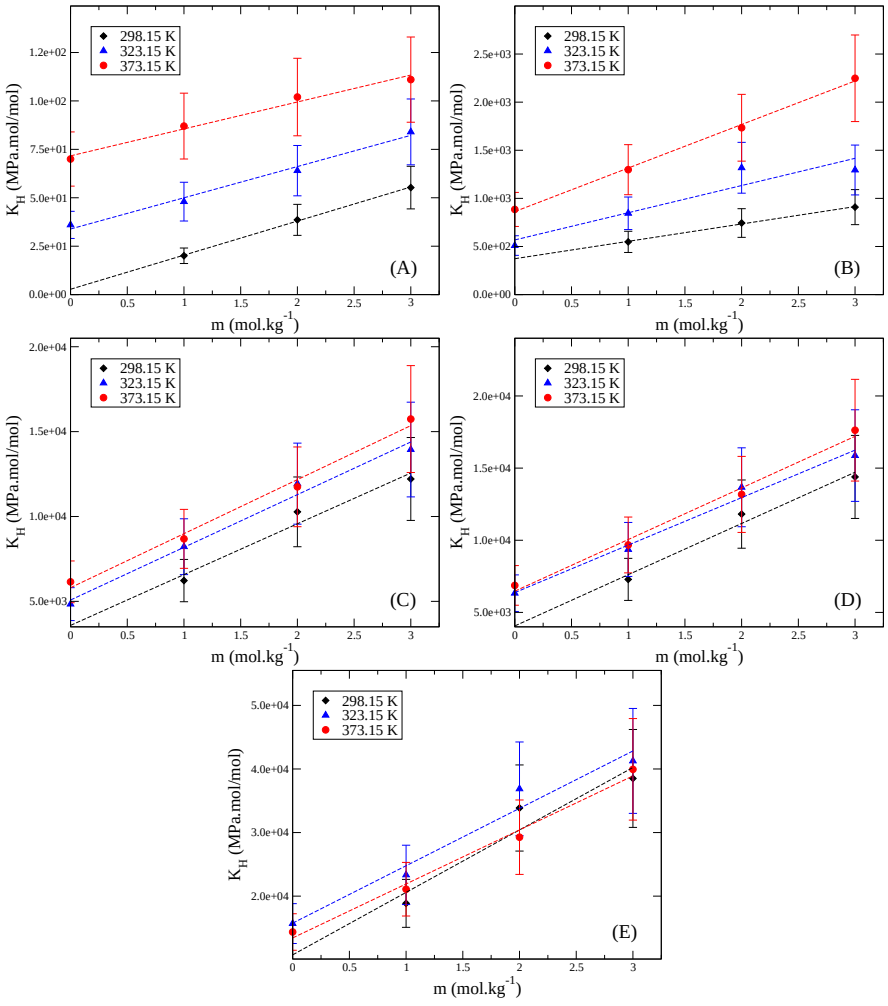

Figure 10: Simulated Henry constant values for SO_2 (A), CO_2 (B), NO (C), O_2 (D), and N_2 (E) in NaCl aqueous solutions as a function of the salt concentration, at 298.15 K (diamonds), 323.15 K (triangles) and 373.15 K (circles).